Experimental measurement of the degree of chaotic synchronization using a distribution exponent

P. Khoury, M. A. Lieberman, and A. J. Lichtenberg
Department of Electrical Engineering and Computer Sciences and the Electronics Research Laboratory, University of California, Berkeley, California 94720
(Received 22 December 1997)

We investigate the use of a distribution exponent for determining the degree of chaotic synchronization of two nearly identical systems. This exponent can be easily measured experimentally; its value corresponds closely to the probability of separation of the two systems, and it is closely connected to the conditional Lyapunov exponent near the threshold of synchronization. The determination of the degree of synchronization by a distribution exponent is illustrated in both experimental and simulated systems of three digital phase locked loops (DPLL's); one chaotic ''feeding'' DPLL is an input to two ''receiving'' DPLL's. We use the relationship between the conditional Lyapunov exponent and the distribution exponent to evaluate a model of our experimental system in which we approximate the feeding chaotic DPLL system with random noise. We determine the degree of synchronization of the two receiving DPLL's by calculating the conditional Lyapunov exponent. The close relationship between the conditional Lyapunov exponent and distribution exponent at the threshold of synchronization allows us to compare our experimental measurements of synchronization, which use the distribution exponent, with the conditional Lyapunov exponents calculated from analysis. [S1063-651X(98)14705-0]

PACS number(s): 05.45.+b, 02.50.Ey

I. INTRODUCTION

A defining characteristic of a chaotic system is that it is sensitive to initial conditions. Two identical chaotic systems that start with different initial conditions will never synchronize. Pecora and Carroll conjectured that a stable subsystem of a chaotic system can synchronize if all conditional Lyapunov exponents of the subsystem are negative, and they demonstrated this numerically for the Lorenz and Rossler systems [1,2]. The results of the simulations were evaluated in two different ways, through the conditional Lyapunov exponents of the subsystem and through examination of the time evolution of the differences between the chaotic system and the subsystem. Pecora and Carroll also demonstrated chaotic synchronization in an experimental system [1,2]. They evaluated the synchronization behavior of the experimental system through examination of the time evolution of phase space differences. Since the differences between the chaotic system and the subsystem decreased to an amount smaller than the scale of the attractor, they concluded that the experimental system synchronized. Further evidence of synchronization was provided by a plot of one variable in the chaotic system versus the similar variable of the subsystem. Two synchronized systems, where one variable is identical to the other, produce a straight line.

Since these two papers, many researchers have further explored and generalized the concept of chaotic synchronization and proposed uses for this phenomenon [3–15]. Pecora and Carroll's initial model of chaotic synchronization was broadened by Rulkov *et al.* [3] to encompass chaotic systems and subsystems which might not be identical. They call this ''generalized synchronization,'' and showed how to detect it even when two signals exhibit large differences. They also developed a new way of detecting generalized synchronization using auxiliary systems [4]. Kim [5] investigated the link between on-off intermittency and chaotic synchronization. Carroll, Heagy, and Pecora studied how the chaotic signal transmitted between system and subsystem can be transformed while still maintaining chaotic synchronization [6]. Vieira, Lichtenberg, and Lieberman [10] showed that the concept of synchronized chaos could be extended to discrete systems. Many studies of chaotic synchronization have focused on the potential use for secure communication [7–14]. These studies required evaluation of whether two systems are synchronized, which was determined using the original methods of Pecora and Carroll.

The most widely used method for examining synchronization is a plot of a one variable of the chaotic system versus the same variable of the subsystem [4–11]. For simulations, these plots show synchronization through straight lines which are visually obvious and carry a clear physical meaning. However in experiments, the correlation between two variables is not exact, exhibiting a spread in the differences between variables [11]. This spread arises from the physical differences between the two subsystems being compared, or from noise introduced separately into the two subsystems. Comparing such plots allows a qualitative comparison between synchronized and unsynchronized states, but does not allow a quantification of the differences.

A second method for measuring synchronization is to average the error difference between the two signals and either use this statistic directly or normalize by the overall signal strength to obtain a signal-to-noise ratio [13,14]. This method is quantitative and easy to implement. However, it does not uniquely measure the degree of synchronization. For example, two systems which are strongly synchronized but have large system differences may have an average error, which is the same as two systems which are weakly synchronized but have smaller system differences.

In addition to using a straight line synchronization plot, the authors of Ref. [6] used the conditional Lyapunov exponent to evaluate the degree of chaotic synchronization. If the sign of the largest conditional Lyapunov exponent is negative, then the system is synchronized. Reference [6] also used the magnitude of the largest conditional Lyapunov exponent as an indication of the degree of synchronization. The authors determined these exponents numerically from the equations of motion. It is difficult to calculate the conditional Lyapunov exponent from experimental data [16].

Pikovsky [17] introduced the concept of a distribution exponent, which is the ratio of the logarithm of probability versus the logarithm of separation, to evaluate synchronization of orbits of a simple mapping subject to noise. The sign of the exponent indicates whether or not the two systems are synchronized, and the magnitude is a measure of the degree of synchronization. We explored the use of the distribution exponent to characterize orbit synchronization of mappings for more general noise distributions [15]. We showed that this method for evaluating synchronization is related to other methods. The mean error difference can be calculated once the probability distribution is known. More important, the Lyapunov exponent and the distribution exponent change sign together. When the distribution exponent equals zero the Lyapunov exponent also equals zero, which is the threshold of synchronization. The distribution exponent is easier to measure than the Lyapunov exponent in an experiment, and the Lyapunov exponent is easier to determine in analyzing known equations.

Kuramoto and Nakao [18] studied a large array of identical systems all driven by random forcing which varied slowly across the array. Interested in self-similarity across this array, they developed equations predicting the probability distribution of separation between two nearby neighbors that are similar to ours in Ref. [15]. From the distribution, they predicted the moments of the distribution and how these moments vary across the array. Both of these predictions were confirmed through simulations.

In this paper we describe experimental measurements of synchronization using a system of three digital phase locked loops (DPLL's). The circuits were directly connected to a data acquisition board to make measurements of circuit dynamics. Digital phase locked loop dynamics have been extensively studied, so their dynamics is well known [10,11,19–21]. These dynamics are well described by a mapping equation which allows us to perform accurate and fast simulations of the DPLL systems we study. In addition, DPLL systems have been used in many applications such as clock synchronization and random number generation [19,21].

In Sec. II, we review the results of previous work necessary for the present study. In Sec. III, we describe the dynamics of an individual DPLL, and of the experimental system of a chaotic DPLL feeding two nearly identical DPLL's. In Sec. IV, we describe the experiment and how the experimental data was taken and processed to produce probability plots of separation of the DPLL outputs. The values for distribution exponent are measured from these plots and compared to DPLL simulations, for which conditional Lyapunov exponents are also measured. In Sec. V, we develop an analytical model of our experimental system which we test by comparing the threshold of synchronization measured by the distribution exponent in the experiment to the threshold of synchronization measured by the Lyapunov exponent in the model. We show how noise can be used to approximate chaos in the model of our experimental system, and how Fourier methods can be used to analyze the result. From the results, we calculate the Lyapunov exponent and compare the threshold of synchronization to that found in our experiment. We determine the relationship between the distribution exponent and the conditional Lyapunov exponent near the threshold of synchronization.

II. MEASURES OF SYNCHRONIZATION

Two identical maps h with different state variables w and x, with the same additive noise ξ, but with a small difference noise δ,

$$w_{n+1}=h(w_n)+\xi_n+\frac{\delta_n}{2} \tag{1}$$

and

$$x_{n+1}=h(x_n)+\xi_n-\frac{\delta_n}{2} \tag{2}$$

have a separation $r_n=w_n-x_n$. We use a logarithmic separation scale to characterize the degree of synchronization:

$$z_n=\ln|r_n|. \tag{3}$$

By assuming small separations, but large compared to δ, we developed equations in a previous paper [15] which describe the evolution of the small separations. The increase or decrease of the separation is related to the average state $s_n=(w_n+x_n)/2$ by

$$z_{n+1}=z_n+\ln|h'(s_n)|. \tag{4}$$

The same map which describes the individual dynamics of Eqs. (1) and (2) also approximately governs the average dynamics for nearly synchronized systems,

$$s_{n+1}=h(s_n)+\xi_n. \tag{5}$$

The instantaneous Lyapunov exponent, which describes the change in separation during one time step, is given by

$$\Lambda_n^1=\ln|h'(s_n)|. \tag{6}$$

The average of the instantaneous Lyapunov exponent over a typical trajectory of s_n is the conditional Lyapunov exponent

$$\lambda=\lim_{N\to\infty}\frac{1}{N}\sum_{n=0}^{N}\Lambda_n^1. \tag{7}$$

It is a measure of the average rate that two nearby systems in phase space separate or approach. If the conditional Lyapunov exponent is negative, the two noisy systems on average approach one another and will synchronize. If the conditional Lyapunov exponent is positive, the two noisy systems separate from each other on average and will not

synchronize. Definition (7) can be extended to a map $s_{n+1}=h(s_n,y_n)$, fed by a chaotic signal y, by defining

$$\lambda=\lim_{N\to\infty}\frac{1}{N}\sum_{n=0}^{N}\ln\left|\frac{\partial}{\partial s}h(s_n,y_n)\right|, \tag{8}$$

where s_n and y_n are chaotic trajectories of the entire system.

As in our previous paper we use definitions (7) and (8) to make theoretical predictions about the synchronization behavior of two systems subject to noise or chaotic inputs. These definitions are only useful if there is complete and accurate knowledge of the synchronization system. Then simulations of one map yield the conditional Lyapunov exponent and a prediction as to whether two systems will synchronize or not. Such theoretical predictions were made by Pecora and Carroll, who also performed experiments proving the link between the sign of the conditional Lyapunov exponent and synchronization [1,2]. The magnitude of the conditional Lyapunov exponent gives the rate of separation or approach, and therefore quantifies synchronization. Systems with a large negative conditional Lyapunov exponent synchronize rapidly. Similarly, a large positive conditional Lyapunov exponent indicates rapid desynchronization. Since measuring the magnitude of the conditional Lyapunov exponent in a synchronizing experiment is difficult, we determine the degree of synchronization through the distribution exponent (defined below), which is related to the Lyapunov exponent [15]. We showed in Ref. [15] that an invariant distribution exists for r, and that the distribution took the form of a truncated geometric probability,

$$f_R(r)\propto r^{\sigma-1}\quad r_s<r<r_l, \tag{9}$$

with other behavior at small separations r_s and at large separations r_l. The transformation of this distribution to a logarithmic measure of separation creates an invariant distribution which has a truncated exponential form,

$$f_Z(z)\propto e^{\sigma z}\quad z_s<z<z_l. \tag{10}$$

A plot of the logarithm of probability versus the logarithm of separation has a linear region where Eq. (10) holds.

An example taken from our previous paper illustrates the behavior of Eq. (10) using a piecewise linear map

$$h(x)=\begin{cases}\left(\dfrac{-m_s+3}{2}\right)x-\dfrac{m_s}{4}+\dfrac{1}{4}, & x<\dfrac{1}{6}\\[2ex] m_s x, & -\dfrac{1}{6}\leqslant x<\dfrac{1}{6}\\[2ex]\left(\dfrac{-m_s+3}{2}\right)x+\dfrac{m_s}{4}-\dfrac{1}{4}, & \dfrac{1}{6}\leqslant x,\end{cases} \tag{11}$$

with additive Gaussian white noise ξ on the circle, so that mappings (1) and (2) are taken mod 1. The synchronization of these maps depends on the parameter m_s and the variance of the noise ξ. We plot the logarithm of probability versus the logarithm of separation for maps (1) and (2) using mapping (11) in Figs. 1(a)–1(c) for different parameters m_s and noise variances. Each graph has a middle region marked by a straight line of slope σ. Figure 1(a), containing a positively sloped line, has a greater probability weight toward larger separations, indicating that the two systems are unsynchronized. Figure 1(b), with a negative slope, implies that the maps are synchronized because the probability distribution is weighted towards smaller separations. Figure 1(c), with a nearly zero slope, shows two maps on the border between synchronization and desynchronization. We identify the slope of the line, the distribution exponent σ, as a measure of synchronization.

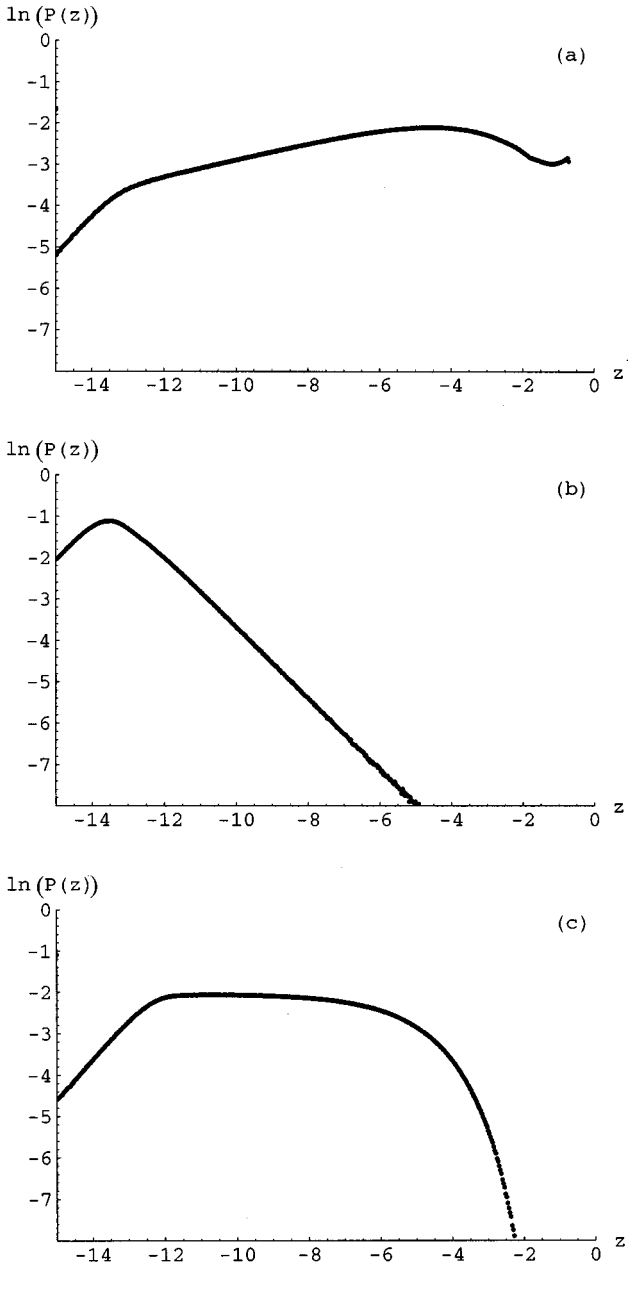

FIG. 1. Typical probability distributions of the separation of two nearly identical maps. The probability and the separation are on logarithmic scales. (a) Unsynchronized. (b) Synchronized. (c) Threshold of synchronization.

The three figures show deviations from geometric (straight line) behavior, with decreases in probability toward small and large scales. The decrease on the right beyond z_l (or r_l) is produced by the finite size of the system orbits.

Nonlinear terms modify Eqs. (4) and (5) to keep the system bounded, as the separation cannot exceed the system size. The exponential region is bounded on the left by z_s (or r_s) due to the small noise and parameter differences between the two systems.

To examine the role of differences at the lower boundary, we analyze noise differences and then show that parameter differences behave similarly to noise differences. These differences only become important when the separation between the two systems is sufficiently small. Consider the case of no separation $r_n=0$. Two identical states acted on by two systems with small difference noise δ will separate by

$$r_{n+1}=\delta_n. \tag{12}$$

The separations between the pairs of systems shown in Fig. 1 are never exactly zero, but, when $z<z_s$, the magnitude of the difference noise δ is larger than the separation r between the two systems and Eq. (12) will hold approximately. The difference noise forces a finite separation of the two systems and the boundaries r_s and z_s are directly proportional to δ.

Differences between the two systems due to differences in parameters can also be considered as a form of difference noise [17]. Consider two systems containing a parameter α which differs in each system by a small amount ε,

$$w_{n+1}=h(w_n,\alpha+\varepsilon)+\xi_n \tag{13}$$

and

$$x_{n+1}=h(x_n,\alpha-\varepsilon)+\xi_n. \tag{14}$$

Since ε is small, we can expand h around α:

$$w_{n+1}=h(w_n,\alpha)+\xi_n+\frac{\partial}{\partial\alpha}h(w_n,\alpha)\varepsilon \tag{15}$$

and

$$x_{n+1}=h(x_n,\alpha)+\xi_n-\frac{\partial}{\partial\alpha}h(x_n,\alpha)\varepsilon. \tag{16}$$

Because the third terms in Eqs. (15) and (16) are not constant but instead depend on the random variables w_n and x_n, they act like a difference noise δ.

Besides deriving the form of the probability distributions, we also demonstrated in Ref. [15] that the conditional Lyapunov exponent and the distribution exponent change sign together, establishing a correspondence between the two measures of synchronization. All the calculations were for maps with additive noise. We also showed synchronization plots for two nearly identical maps fed with chaos. They exhibited the same general bounded exponential probability distribution behavior, and we hypothesized that the distribution exponent could also be used to measure the synchronization behavior of chaotically fed systems. We examine this hypothesis here, by obtaining probability plots from a chaotic experimental system. These experimental probability plots exhibit the same bounded exponential distribution behavior.

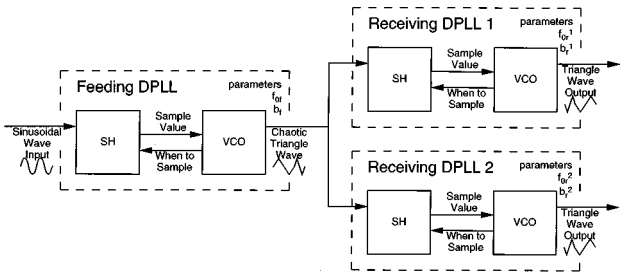

FIG. 2. Experimental system of DPLL's.

III. DIGITAL PHASE LOCKED LOOPS

We use a system of three first order DPLL's connected as shown in Fig. 2 to study synchronization experimentally. Each DPLL contains two components; a voltage controlled oscillator (VCO) and a sample and hold (SH) amplifier. The first DPLL is fed by a sine wave, and the second two are fed by the oscillating output of the first DPLL. Let $g(t)$ represent the incoming signal. The SH component takes a sample Ψ_n of the incoming signal at time t_n:

$$\psi_n=g(t_n). \tag{17}$$

The value of this sample controls the behavior of the VCO. The VCO oscillates at a frequency proportional to the sampled voltage,

$$f=f_0(1+b\psi). \tag{18}$$

This oscillation is often modeled to be sinusoidal, but in an experimental system it is more likely to be either a square or triangular wave. A new sample is taken by the SH amplifier after the VCO completes one full oscillation. The time between samples is $1/f$, and the new sample time is

$$t_{n+1}=t_n+\frac{1}{f_0(1+bg(t_n))}, \tag{19}$$

which describes the dynamics of the DPLL. We consider the case where the incoming signal $g(t)$ is a sinusoid with time normalized so that the oscillation frequency is unity. Now the dynamics of the DPLL is fully described by the mapping equation

$$t_{n+1}=t_n+\frac{1}{f_0(1+b\ \sin(2\pi t_n))}. \tag{20}$$

Because $g(t)$ is periodic with unit period, the times t_n separated by integers are equivalent states, which we transform into the phase variable $\phi_n=t_n \bmod 1$, giving

$$\phi_{n+1}=\phi_n+\frac{1}{f_0(1+b\ \sin(2\pi\phi_n))}. \tag{21}$$

A study of Bernstein [21] explored the dynamics of this system, the boundary of invertibility, and the regions of regular and chaotic behavior. Figure 3 shows the regions of regular and chaotic behavior by plotting the Lyapunov exponents obtained from simulations of Eq. (21) over the (f_0,b) parameter plane. We operate our first (''feeding'') DPLL at a chaotic point in parameter space, $f_{0f}=0.714$ and $b_f=0.28$.

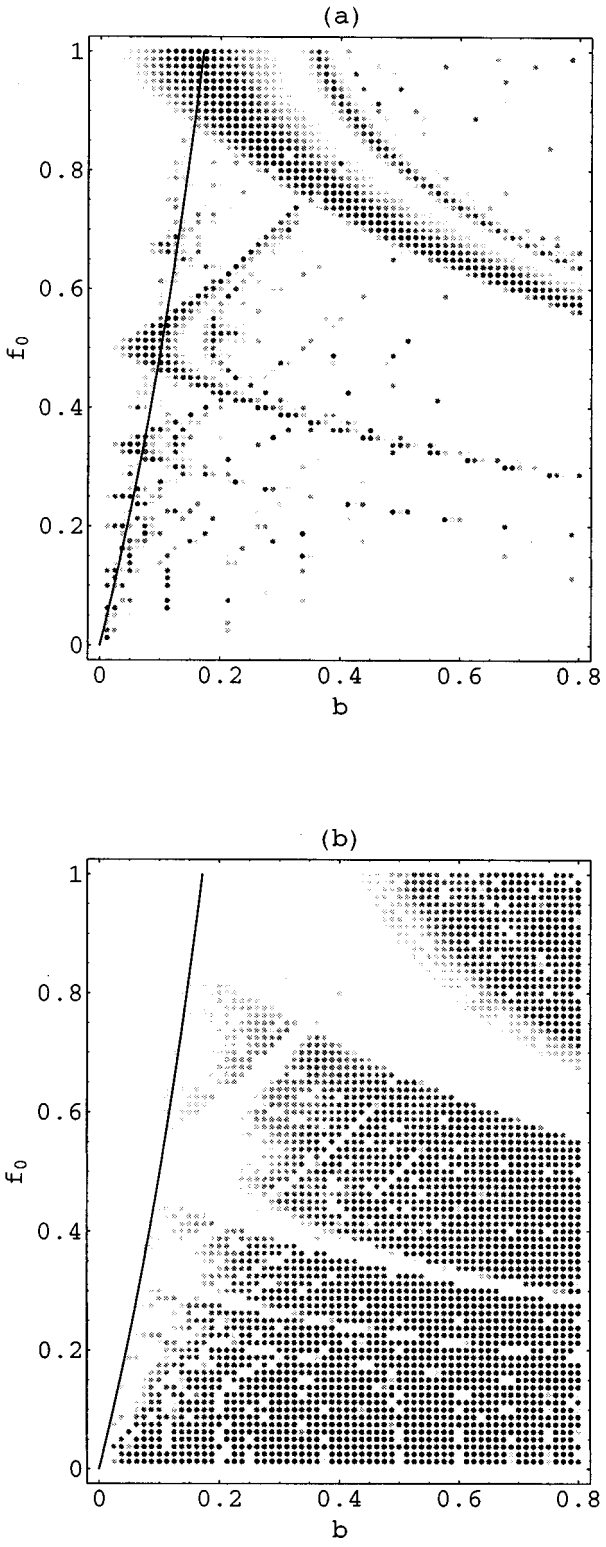

FIG. 3. Parameter space stability diagram of a first order DPLL with sinusoidal input. (a) Negative Lyapunov exponents. (b) Positive Lyapunov exponents. The darker the dot, the larger the magnitude of the Lyapunov exponent.

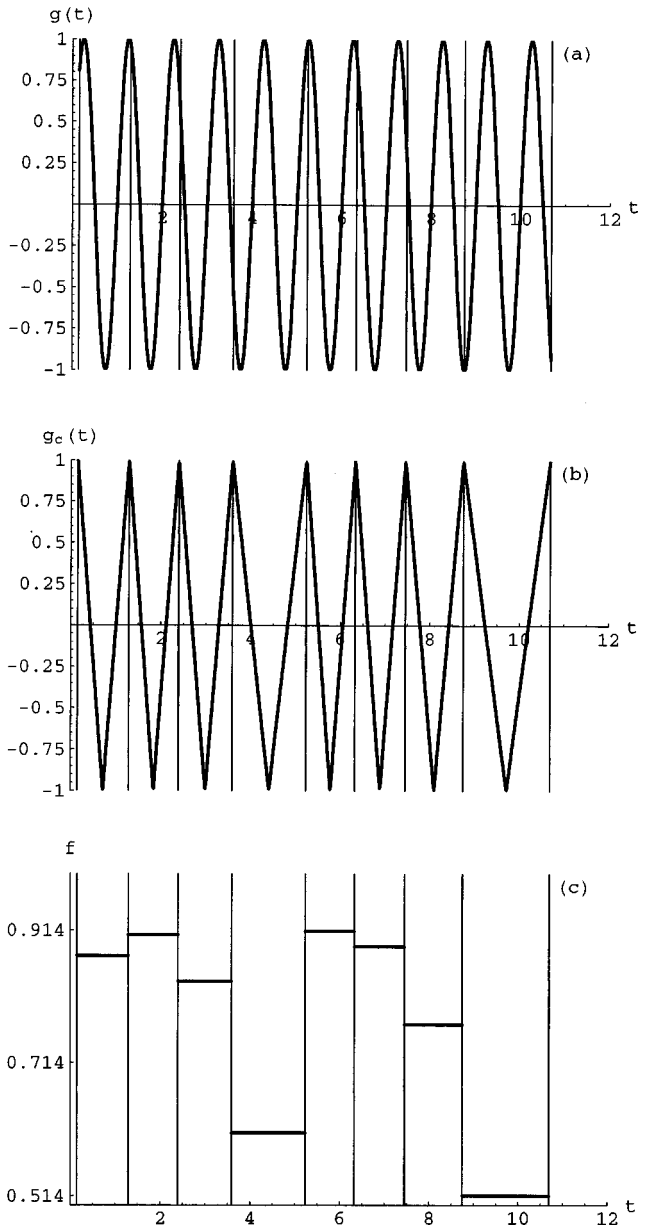

FIG. 4. The typical dynamics of a first order DPLL with parameters $f_0=0.714$ and $b=0.28$. (a) Sinusoidal input. (b) Typical output of the DPLL. (c) Frequency of the DPLL output. The three values labeled on the vertical axis are $f_0(1-b_{\max})$, f_0, and $f_0(1+b_{\max})$, respectively. Vertical lines show the sampling times, at which the DPLL changes to a new frequency.

In Fig. 4(a), we mark sampling times (vertical lines) on the sinusoidal input to the DPLL, which occur at the maximum of the VCO output. The VCO output $g_c(t)$ is a triangular wave as shown in Fig. 4(b). Figure 4(c) shows how the frequency of $g_c(t)$ changes in a discrete way to a new frequency at the beginning of each oscillation period. The invariant distribution of these frequencies is shown in Fig. 5. This distribution is fractal because of the chaotic nature of the system. From the frequency of $g_c(t)$, we can determine the phase of the signal:

$$\theta(t)=\left(\int_0^t f(t')dt'+\theta(0)\right)\bmod\ 1. \tag{22}$$

Because the frequency stays fixed for an entire oscillation the discontinuities in phase only occur at one particular phase value which we define to be zero, when the DPLL takes a sample. The two ''receiving'' DPLL's are fed by the chaotic

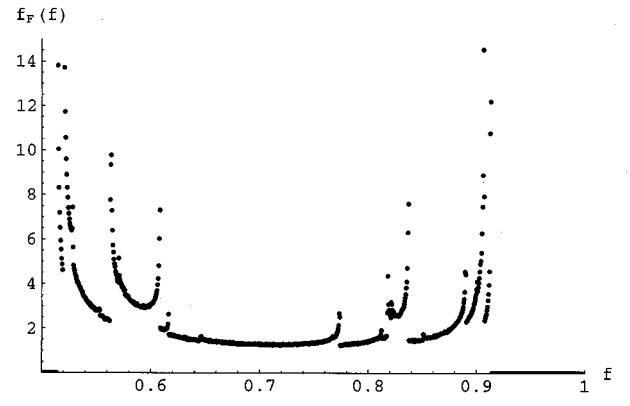

FIG. 5. Probability density of the frequency of a DPLL output.

signal $g_c(t)$. These DPLL's have parameters (f_{0r}^1, b_r^1) and (f_{0r}^2, b_r^2). In order to study synchronization, we tune the two loops so that $f_{0r}^1 \approx f_{0r}^2 \approx f_{0r}$ and $b_r^1 \approx b_r^2 \approx b_r$. As noted in Eqs. (15) and (16), small parameter differences are modeled through the use of additive difference noise. Each receiving DPLL is described by Eq. (19), with $g_c(t)$ as input for both and with difference noise $\delta/2$ added to one equation and subtracted from the other:

$$t_{n+1}^1 = t_n^1 + \frac{1}{f_{0r}(1 + b_r g_c(t_n^1))} + \frac{\delta_n}{2}, \tag{23}$$

$$t_{n+1}^2 = t_n^2 + \frac{1}{f_{0r}(1 + b_r g_c(t_n^2))} - \frac{\delta_n}{2}. \tag{24}$$

IV. EXPERIMENT

Appendix A contains a description of our experimental realization of Eqs. (23) and (24). In the experimental system the circuits making up the two DPLL's are not exactly identical. One limiting factor is that the VCO's contained in each circuit have slight nonlinearities which differ from each other. It is also difficult to tune the parameters f_{0r} and b_r to be identical in the two circuits. A typical plot of the voltage versus frequency characteristics of one DPLL is shown in Fig. 6(a), and the typical error between two of them is shown in Fig. 6(b). The error is measured as the difference between the frequencies produced by each VCO divided by the average frequency of the two VCO's. Also marked on the plot is the center frequency f_0 and the range of frequencies used in our experiment. We were able to make the two DPLL's similar to one part in one thousand. We model the differences between the two systems in our simulations with a difference noise δ that is white and uniformly distributed between -0.001 and $+0.001$.

We determine differences between the dynamics of the two receiving loops experimentally by measuring the sampling times t_n^1 and t_n^2. We define the difference between the two loops to be the time difference between one sample and its nearest neighbor in the other loop's sample space:

$$r(t_n^1) = \min_m(|t_n^1 - t_m^2|) \tag{25}$$

and

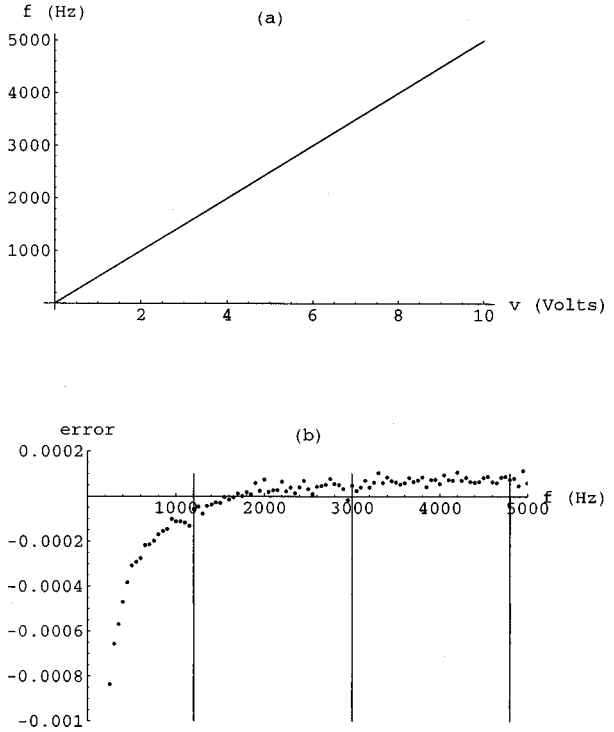

FIG. 6. Plot (a): the frequency voltage characteristic for the VFC320. Plot (b): the frequency error as a function of frequency as measured between two VFC320's tuned to have nearly identical frequency voltage characteristics. The region between the leftmost and rightmost vertical lines shows the greatest frequency range of ''receiving'' DPLL operation.

$$r(t_n^2) = \min_m(|t_n^2 - t_m^1|). \tag{26}$$

The time differences are measured in increments of a 10-MHz clock used by our data acquisition board. The highest frequency of our receiving loops is 4800 Hz, making our measurement resolution at worst 5×10^{-4}.

We take 10 000 time samples for each receiving loop, and convert this data into a probability distribution. At every sample time we determine the difference between the two loops and order this list of differences from smallest to largest. Let $N_{\leqslant}(r)$ represent the number of separations in this list less than or equal to the separation r. Let N_t be the total number of separations in the list. If $P(\bullet)$ represents the probability of some event, and R is the random variable representing the separation, then

$$F_R(r) \equiv P(R \leqslant r) = \frac{N_{\leqslant}(r)}{N_t} \tag{27}$$

represents the probability that any particular sample of one loop will be within r clock ticks of a sample by the other loop.

Through the equality in Eq. (27), we generate an approximate cumulative distribution function $F_R(r)$ [22]. This function is discrete in both separation and probability, increasing in multiples of $1/N_t$ at integer values which represent multiples of the 10-MHz clock. Figure 7 shows a representative cumulative distribution function. We take the logarithm of

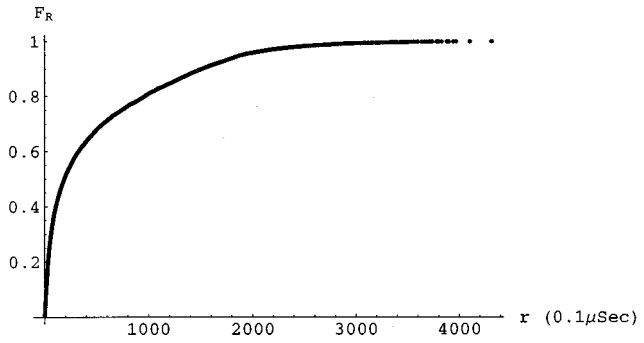

FIG. 7. Cumulative distribution $F_R(r)$ of separation times measured by 10-MHz clock ticks.

the abscissa of this function to generate a cumulative distribution of the logarithm of the separation probability. If

$$Z=\ln(R), \tag{28}$$

then

$$F_Z(z)=P(Z\leqslant z)=P(\ln(R)\leqslant z)=P(R\leqslant e^z)=F_R(e^z). \tag{29}$$

The derivative of the cumulative distribution function yields the probability density function [22]

$$f_Z(z)=\frac{d}{dz}F_Z(z), \tag{30}$$

where

$$f_Z(z)dz=P(z<Z\leqslant z+dz) \tag{31}$$

is the function used in Eq. (10) to describe the distribution exponent. Since we have a discrete approximation to the cumulative distribution function $F_Z(z)$, we take the derivative of this function numerically. We find the derivative at a discrete point on the cumulative distribution function by taking that point and its two adjacent points, constructing an approximate polynomial between these points, and taking the derivative of the polynomial at the center point. We approximate the derivative at every data point along the cumulative distribution function. To see more clearly the exponential region, we take the logarithm of the numerical derivatives which estimate the density function $f_Z(z)$. Figure 8 shows the logarithm of the transformation by Eqs. (29) and (30) of the data shown in Fig. 7. Figure 8 is noisy because of the relatively small size of our data set. To smooth it, we sweep a window of width 0.5 (in z) across the figure computing the running average of all values which lie within the window. Typical results of this averaging is shown in Fig. 9.

The logarithmic scale for f in Fig. 9 makes the bounded exponential behavior in the experimental probability distribution stand out as a linear region in the plot. Similar to Fig. 1, this linear region gives an application of the analysis of our previous paper [15] to an experimental system. We use the slope of the linear region, which is the distribution exponent, as a measure of the degree of synchronization. The results shown in Fig. 9 describe an experimental system on the threshold between synchronization and desynchronization. This figure is obtained strictly from experimental data.

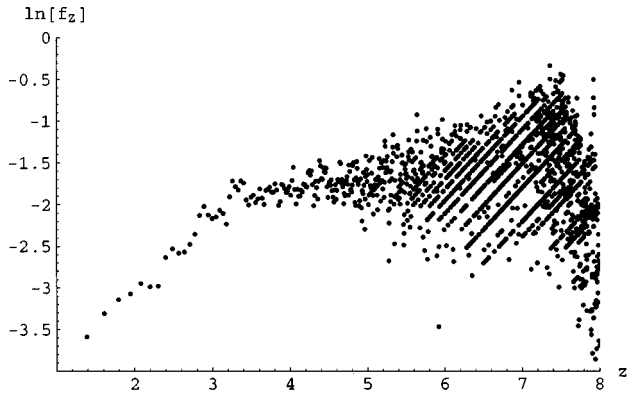

FIG. 8. Logarithm of the approximate derivative of the cumulative distribution $F_Z(z)$.

The measurements and the transformation of the experimental data are more straightforward than estimating the Lyapunov exponent from experimental data [16].

The experimental figure is also analogous to Fig. 1 at the boundaries of the exponential region. The probability density decreases rapidly as separations increase to near the system size. The probability density also decreases rapidly as separations become smaller than the magnitude of the effective difference noise. Note that the magnitude of the effective difference noise in the experimental system is larger than that in the simulated mapping system, and therefore the exponential region is smaller in Fig. 9 than in Fig. 1.

We have determined the synchronization behavior and carried out quantitative synchronization surveys in the parameter space of our two receiving DPLL's. We expect the synchronization behavior of the receiving DPLL's to change as the parameters f_{0r} and b_r are varied. We use the distribution exponent to measure the degree of synchronization at many points in parameter space, and make a contour plot of the experimental distribution exponent values σ in Fig. 10. The bold line on this plot is the threshold of synchronization where the distribution exponent σ equals zero. The region to the upper left of this bold line is synchronized and the region to the lower right is unsynchronized, with the contours separated by values of $\sigma=0.25$. The largest distribution exponent present in Fig. 10 is unity. This limit, as shown in Appendix

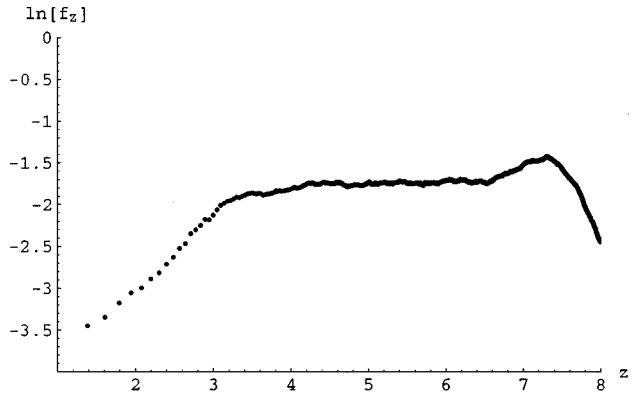

FIG. 9. Running average of the distribution shown in Fig. 8, and an the approximate density function $f_Z(z)$.

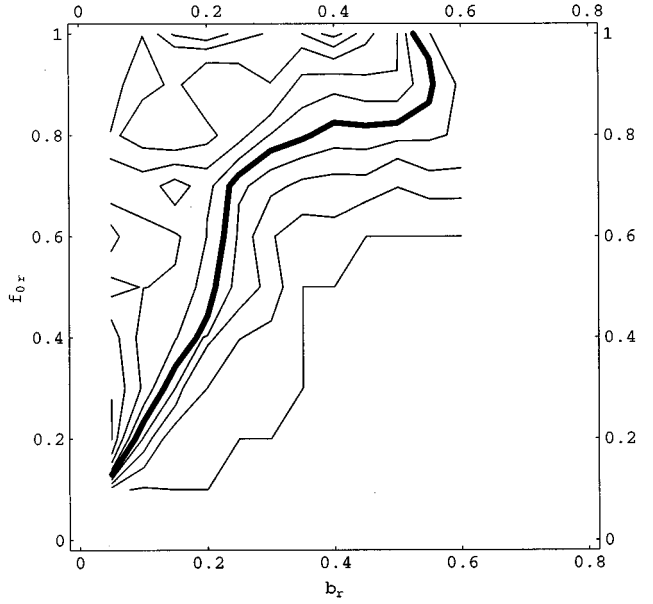

FIG. 10. Contour plot of experimental measurements of the distribution exponent in the $f_{0r}b_r$ parameter plane. The bold contour represents the threshold of synchronization $\sigma=0$. Toward the upper left of the plot, the contour lines represent decreasing values of the distribution exponent and are separated by increments of 0.25. Toward the lower right, the contour lines increase in increments of 0.25.

B, results from our experimental configuration using two receiving loops.

For comparison we plot, in Fig. 11, the distribution exponents as measured through simulations of Eqs. (23) and (24). For the same mapping equations, we can also compute the conditional Lyapunov exponent which is, given in Fig. 12. Since the two measures of synchronization change sign together, those measures should match at the threshold of synchronization $\lambda=\sigma=0$, which can be seen by comparing the bold lines indicating $\sigma=0$ and $\lambda=0$ in Figs. 11 and 12. These curves are qualitatively similar to the experimental curve of $\sigma=0$ in Fig. 10, with some relatively small differences. We can therefore determine synchronization behavior directly from experimental data independent of model equations. In addition, at the threshold of synchronization, measurements of synchronization using the distribution exponent can be compared to determinations of synchronization from model equations using the conditional Lyapunov exponent.

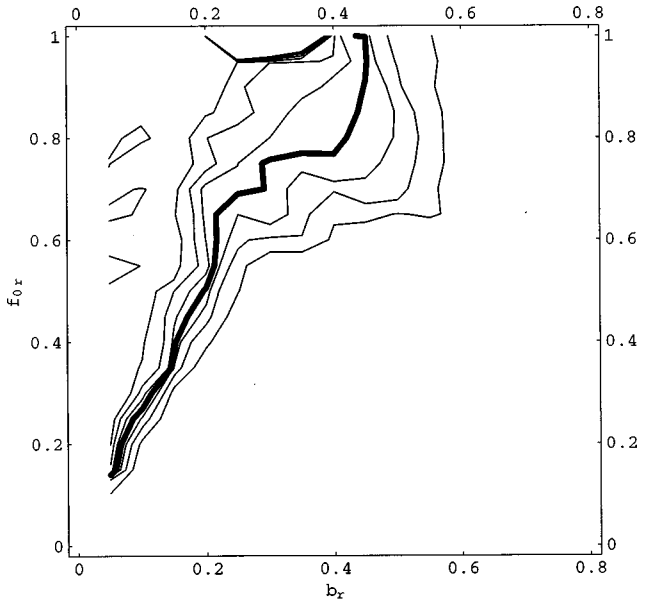

FIG. 11. Contour plot of distribution exponent determined from simulations of the experimental system. The contours change in increments of 0.25, with the bold contour indicating $\sigma=0$.

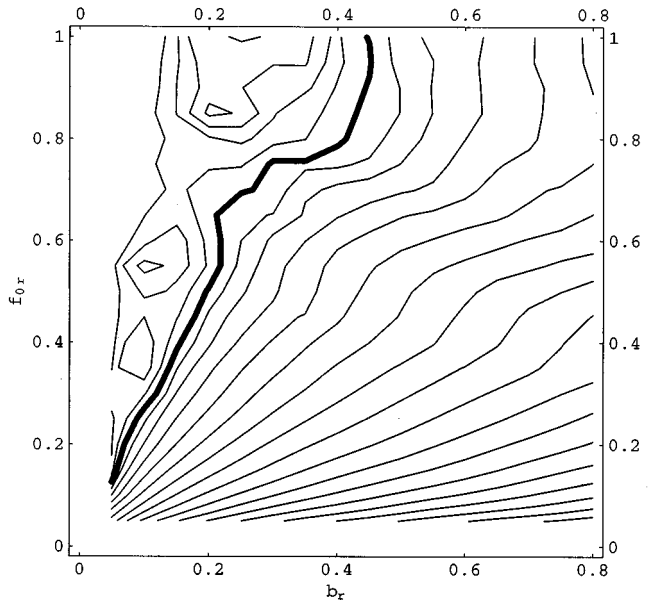

FIG. 12. Contour plot of the conditional Lyapunov exponent determined from computer simulations of the experimental system. The contours change in increments of 0.25, with the bold contour indicating $\lambda=0$.

V. ANALYSIS

We develop a model of our DPLL system using a random feeding signal in place of the chaotic one. In our analysis we calculate the conditional Lyapunov exponent to determine the synchronization behavior of our model, because it is more straightforward than a calculation of the distribution exponent. Despite predicting synchronization behavior through the conditional Lyapunov exponent and measuring synchronization behavior through the distribution exponent, we can compare prediction with experiment near the threshold of synchronization, where they give similar results.

To analyze the synchronization behavior of DPLL's, we model the frequency of the incoming signal $F(t)$ as a random Ornstein-Uhlenbeck process [23]. Using this model the frequency of the signal being received by the DPLL's will always be Gaussian [22]. It is also time invariant, so a constant mean and an autocovariance function $R(t)$ will completely characterize it. The mean f_{0f} of the frequency is chosen to be the same as that of the chaotic feeding signal. In our experimental and simulated systems, the signal fed into the two receiving DPLL's was produced by a sinusoidally driven DPLL with parameters $f_{0f}=0.714$ and $b_f=0.28$. The

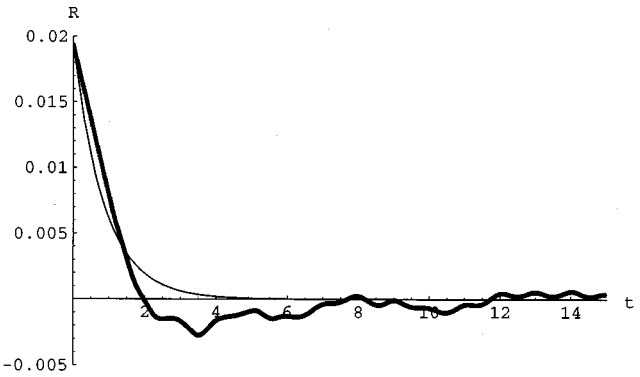

FIG. 13. Autocorrelation plot $R(t)$ of the frequency of the output of the ''feeding'' DPLL (dark curve). The exponential curve (light line) is the best fit to $R(t)$ in the least squares sense as the time constant τ is varied.

frequency distribution of this chaotic signal, shown in Fig. 5, has a mean of $f_{0f}=0.687$.

The autocovariance function depends on the separation in time between two samples, and indicates the covariance between two samples. For the Ornstein-Uhlenbeck process the autocovariance function decays exponentially, so that the frequency between two samples is strongly correlated if the samples are taken close together in time, and weakly correlated if the samples are taken far apart in time. Two parameters are needed to uniquely specify this exponential curve: the variance A and correlation time τ:

$$R(t)=Ae^{-t/\tau}. \tag{32}$$

We set $A=0.0193$, which is the variance of the distribution shown in Fig. 5. The autocovariance function of the chaotic signal we are approximating is shown in Fig. 13; we determine τ by fitting it with an exponential to determine the mean square error best fit correlation time $\tau=0.870$. The exponential associated with this correlation time is also shown in Fig. 13. By integrating the random frequency variable F over time,

$$\Theta(t)=\left(\int_0^t F(t')dt'+\Theta(0)\right)\bmod\ 1, \tag{33}$$

we determine the random variable representing the phase of the feeding signal. The value of the random signal is related to the phase of the random signal through the shape of the ''feeding'' wave form $g_f(\theta)$. In our model

$$g_f(\theta)=\mathcal{T}(\theta)\equiv\begin{cases}1-4(\theta \bmod 1) & 0\leqslant\theta \bmod 1<0.5\\ 3+4(\theta \bmod 1) & 0.5\leqslant\theta \bmod 1<1.\end{cases} \tag{34}$$

The map that evolves the receiving DPLL from a phase sampled on the random input signal to a new phase on the random input signal is a function of the nonrandom (or ''sure'') variable $\theta(0)$. Because the input signal is random, the map returns the random variable Θ. From Eq. (33), Θ is the integral of the Ornstein-Uhlenbeck process over the time Δt between one sample and the next,

$$\Theta=\Delta\Theta+\theta(0)=\int_0^{\Delta t}F(t')dt'+\theta(0). \tag{35}$$

The integral of this process is a Gaussian random variable. We determine the mean and variance of this variable as a function of Δt in Appendix C by using the standard characteristics of the integral of the Ornstein-Uhlenbeck process [23]. These characteristics are a function of f_{0f}, A, τ, and Δt, and the frequency $f(0)$ at the instant of the sample. We take the expectation of the mean and variance over the random frequency variable $F(0)$, so that Θ does not depend on $f(0)$, and determine

$$\langle\Theta(\Delta t)\rangle=\theta+f_{0f}\Delta t, \tag{36}$$

and

$$\langle\Theta(\Delta t)^2\rangle-\langle\Theta(\Delta t)\rangle^2=2A\tau(\Delta t-\tau+\tau e^{-\Delta t/\tau}). \tag{37}$$

From Eq. (19), the relationship between Δt and θ in the receiving DPLL is

$$\Delta t=t_{n+1}-t_n=\frac{1}{f_{0r}(1+b_r\psi_n)}=\frac{1}{f_{0r}(1+b_r g_f(\theta))}. \tag{38}$$

We substitute Eq. (38) into Eq. (36) to determine the mean of the new phase in terms of the previous sample

$$\langle\Theta(\theta)\rangle=\theta+\frac{f_{0f}}{f_{0r}(1+b_r g_f(\theta))}. \tag{39}$$

The variance v of the new phase is found similarly by substituting Eq. (38) into Eq. (37),

$$v(\theta)=2A\tau\left(\frac{1}{f_{0r}(1+b_r g_f(\theta))}-\tau+\tau e^{1/-f_{0r}(1+b_r g_f(\theta))/\tau}\right). \tag{40}$$

Equations (39) and (40) completely describe the stochastic map that models our system. Consider the random variable Θ_n with probability density function $f_{\Theta_n}(\theta)$ mapped by the stochastic map [Eqs. (39) and (40)] to a new random variable Θ_{n+1} with probability density function $f''_{\Theta_{n+1}}(\theta'')$, where the double-primed variables are defined below and in Appendix D. We seek an invariant distribution

$$f_{\Theta_n}(\theta)=f''_{\Theta_{n+1}}(\theta''). \tag{41}$$

The random variables Θ_n and Θ_{n+1} exist on the circle $[-\frac{1}{2},\frac{1}{2})$, and their density functions have domain $[-\frac{1}{2},\frac{1}{2})$. The distributions for Θ_n and Θ_{n+1} in this circular domain can be expressed in terms of Fourier coefficients a_n and b_n, and a''_n and b''_n:

$$f_{\Theta_n}(\theta)=\frac{a_0}{2}+\sum_{n=1}^{\infty}a_n\cos(2\pi n\theta)+\sum_{n=1}^{\infty}b_n\sin(2\pi n\theta), \tag{42}$$

$$f''_{\Theta_{n+1}}(\theta'')=\frac{a''_0}{2}+\sum_{n=1}^{\infty}a''_n\cos(2\pi n\theta'')+\sum_{n=1}^{\infty}b''_n\sin(2\pi n\theta''). \tag{43}$$

If

$$a_n=a''_n \tag{44}$$

and

$$b_n=b''_n, \tag{45}$$

then Eq. (41) will hold, and the invariant distribution will have Fourier coefficients given by Eqs. (44) and (45). In Appendix D, we decompose the map into a nonstochastic and a stochastic steps. Using the nonstochastic step, we transform the Fourier coefficients of $f_{\Theta_n}(\theta)$ into the Fourier coefficients of an intermediate distribution $f'_n(\theta')$. We express the stochastic step by transforming a Gaussian distribution on the real line to a distribution function on the circle:

$$f_{\Xi}(v,\xi)=\sum_{i=-\infty}^{\infty}\frac{1}{\sqrt{2\pi v}}e^{[(\xi+i)^2/2v]}. \tag{46}$$

The Fourier coefficients of Eq. (46) are

$$\xi^a_m(v)=2e^{-2\pi^2m^2v} \tag{47}$$

and

$$\xi^b_m(v)=0, \tag{48}$$

where the superscripts a and b refer to the cosine and sine terms, respectively. Finally, using the stochastic transformation (see Appendix D), we transform the Fourier coefficients of the intermediate distribution to the Fourier coefficients of the final distribution. We find a linear relationship

$$a''_n=t^{aa}_{n0}a_0+\sum_{m=1}^{\infty}t^{aa}_{nm}a_m+\sum_{m=1}^{\infty}t^{ab}_{nm}b_m \tag{49}$$

and

$$b''_n=t^{ba}_{n0}a_0+\sum_{m=1}^{\infty}t^{ba}_{nm}a_m+\sum_{m=1}^{\infty}t^{bb}_{nm}b_m. \tag{50}$$

The coefficients t in Eqs. (49) and (50) are given by integrals (D36)–(D41) derived in Appendix D. Defining the matrix

$$\overrightarrow{f_{\theta_i}}=\begin{bmatrix}a_0\\b_1\\a_1\\b_2\\\vdots\end{bmatrix},\quad \overrightarrow{f''_{\theta_{i+1}}}=\begin{bmatrix}a''_0\\b''_1\\a''_1\\b''_2\\\vdots\end{bmatrix},$$

$$\overrightarrow{\overrightarrow{T}}=\begin{bmatrix}t^{aa}_{0,0} & t^{ab}_{0,1} & t^{aa}_{0,1} & t^{ab}_{1,2} & \cdots\\ t^{ba}_{1,0} & t^{bb}_{1,1} & t^{ba}_{1,1} & t^{bb}_{1,2} & \cdots\\ t^{aa}_{1,0} & t^{ab}_{1,1} & t^{aa}_{1,1} & t^{ab}_{1,2} & \cdots\\ t^{ba}_{2,0} & t^{bb}_{2,1} & t^{ba}_{2,1} & t^{bb}_{2,2} & \cdots\\ \vdots & \vdots & \vdots & \vdots & \ddots\end{bmatrix}, \tag{51}$$

we can express Eqs. (49) and (50) in the compact form

$$\overrightarrow{f''_{\theta_{i+1}}}=\overrightarrow{\overrightarrow{T}}\cdot\overrightarrow{f_{\theta_i}}. \tag{52}$$

The Fourier vector $\overrightarrow{f_{\theta_i}}$ and its associated density function will be invariant when

$$\overrightarrow{f''_{\theta_{i+1}}}=\overrightarrow{f_{\theta_i}}. \tag{53}$$

The invariance will exist if the matrix $\overrightarrow{\overrightarrow{T}}$ has an eigenvalue equal to unity. The vector associated with the unity eigenvalue contains the Fourier coefficients of the invariant density function. We can use these coefficients to reconstruct the density function through Eqs. (42) or (43).

We choose where to truncate the infinite matrix $\overrightarrow{\overrightarrow{T}}$ by first noting that accurate approximations of narrow density functions by a Fourier series requires large numbers of coefficients. The smallest variance $v_{\min}$ of Eq. (40) sets a lower bound to the width of the invariant distribution, and we limit the size of the infinite matrix based on the distribution (46) with parameter $v_{\min}$. If we choose to limit the length of $\overrightarrow{f_{\theta_i}}$ to N, where N is the smallest integer, such that

$$0.01\geqslant\xi^a_N(v_{\min})=2e^{-2\pi^2N^2v_{\min}}, \tag{54}$$

we are guaranteed that any density function coefficients greater than N will represent less than 1% of overall probability. We illustrate the procedure for a system with a random frequency triangular input signal

$$g_f(\Theta(t))=\mathcal{T}(\Theta(t)) \tag{55}$$

in which $\Theta(t)$ is the integral of the Ornstein-Uhlenbeck process with parameters $A=0.0193$ and $\tau=0.870$, and with a receiving DPLL having parameters $f_{0r}=0.85$ and $b_r=0.45$. The minimum of Eq. (40) for this set of parameters is

$$v_{\min}=0.018. \tag{56}$$

Using Eq. (54), we determine that the fourth Fourier coefficient of the noise never exceeds 0.01. We choose vectors f which have nine components. Using numerical integration and Eqs. (D36)–(D41), we calculate $\overrightarrow{\overrightarrow{T}}$, and determine its eigenvalues to be

$$\{1,0.434,-0.0036+0.046i,-0.0036-0.0046i,-0.0063,$$
$$-0.0021,-0.0015,<10^{-4},<10^{-4}\}. \tag{57}$$

The eigenvector associated with the eigenvalue 1 is

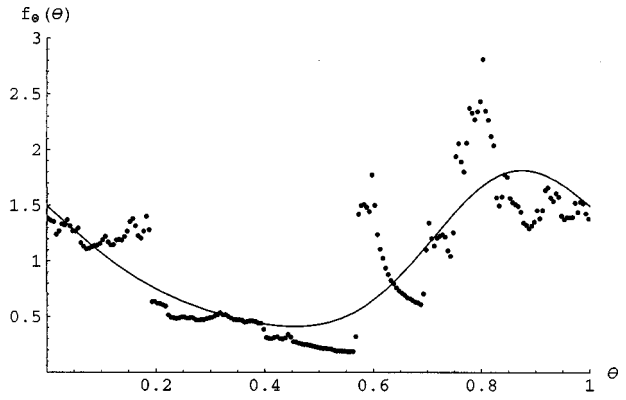

FIG. 14. The solid curve is the invariant probability density function of the phase sampled by a DPLL with parameters $f_{0r}=0.85$ and $b_r=0.45$ receiving a random frequency signal, which is Ornstein-Uhlenbeck process $f_{0f}=0.687$, $A=0.0193$, and $\tau=0.870$. Computer simulation of the density function is indistinguishable from the solid curve. The dotted curve is the invariant distribution of the phase sampled by a DPLL with parameters $f_{0r}=0.85$ and $b_r=0.45$ receiving a chaotic signal. The chaotic signal is produced by a ''feeding'' DPLL with parameters $f_{0r}=0.714$ and $b_r=0.28$ fed by a regular sinusoidal signal with frequency 1.

$$\vec{f}_{\text{invar}}=[2,-0.401,0.0547,-0.136,-0.036,-0.001,-0.015,0.001,0]. \tag{58}$$

We use these Fourier coefficients and Eq. (42) to determine the invariant distribution function shown as the solid line in Fig. 14. The invariant distribution of a simulation of the same system cannot be distinguished from the solid line in Fig. 14. The parameters of the random process were the best fit model for a feeding signal from a chaotic sinusoidally fed DPLL. For comparison we also plot, as dots in Fig. 14, the invariant distribution of a simulation of the chaotically fed DPLL system. We find it easiest to determine the synchronization behavior of the randomly fed system analytically through the conditional Lyapunov exponent. This exponent depends only on an invariant distribution, while analytical calculation of the distribution exponent requires an explicit knowledge of the evolution of the system over time. The conditional Lyapunov exponent λ is a weighted average of the instantaneous Lyapunov exponent Λ^1. For the random frequency map,

$$\Lambda^1(\theta)=\ln\left(\left|\frac{d}{d\theta}\langle\Theta(\theta)\rangle\right|\right), \tag{59}$$

and, for the deterministic chaotic map,

$$\Lambda^1(\phi_n)=\ln\left(\left|\frac{d\phi_{n+1}}{d\phi_n}\right|\right). \tag{60}$$

These expressions are the same, so that

$$\Lambda^1(\theta)=\ln\left(\left|1-\frac{f_{0f}b_r\mathcal{T}'(\theta)}{f_{0r}(1+b_r\mathcal{T}(\theta))^2}\right|\right). \tag{61}$$

To calculate the conditional Lyapunov exponent, we take the expectation of Λ^1 over the invariant distribution

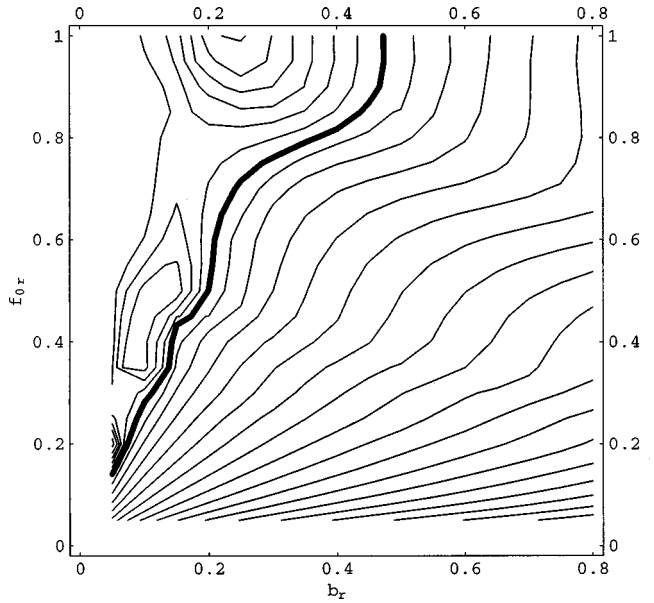

FIG. 15. Contour plot of conditional Lyapunov exponent determined analytically, from invariant distributions. The contours change in increments of 0.25, and the bold contour line identifies $\lambda=0$.

$$\lambda=\int_{-1/2}^{1/2}\Lambda^1(\theta)f_\Theta(\theta)d\theta, \tag{62}$$

Numerical integration of Eq. (62) using the invariant distribution shown in Fig. 14 gives $\lambda=0.0737$. The simulation of the deterministic chaotic system gives $\lambda=0.0879$. We repeat the process of calculating approximate invariant distributions and evaluating Eq. (62) at many points in the $f_{0r}b_r$ parameter plane to obtain the contour plot of the conditional Lyapunov exponent shown in Fig. 15, which can be directly compared with Fig. 12 produced by simulation. Unlike the simulation in which we can also measure the distribution exponent to obtain the contour plot Fig. 11, which can be directly compared to our experimental Fig. 10, we cannot produce a contour plot of distribution exponent from our analysis. Even though we cannot easily predict the distribution exponent, and cannot easily measure the conditional Lyapunov exponent, we can make direct comparisons between the bold lines in Figs. 10 and 15 because the two measures are identical at the threshold of synchronization. Through this method, we conclude that our model is a good approximation of the experiment.

If we define local Lyapunov exponents to be the running average of the instantaneous Lyapunov exponents

$$\Lambda_j^N=\frac{1}{N}\sum_{n=j}^{j+N-1}\Lambda_n^1, \tag{63}$$

and then define the limiting variance v of local Lyapunov exponents to be

$$v=\lim_{N\to\infty} N\ \text{var}(\Lambda^N), \tag{64}$$

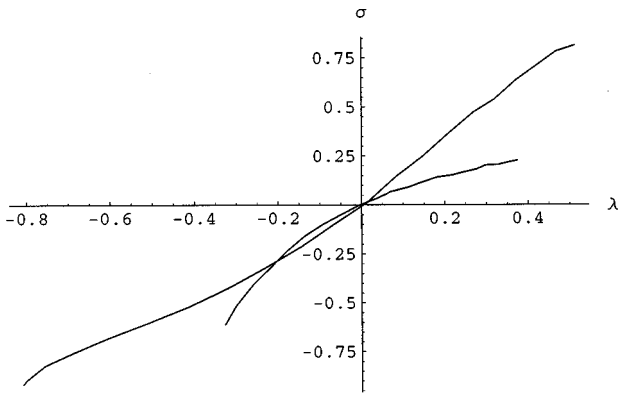

FIG. 16. Plot of the distribution exponent vs the conditional Lyapunov exponent. Both exponents were measured from simulations of ''receiving'' DPLL's fed by Ornstein-Uhlenbeck random frequency processes. The longer path fixes $f_{0r}=0.35$ and varies b_r, while the shorter line fixes $f_{0r}=0.75$ and varies b_r.

the distribution exponent σ is related to the conditional Lyapunov exponent λ near the threshold of synchronization by [15]

$$\sigma=\frac{2\lambda}{v}. \tag{65}$$

We determine how the distribution exponent varies with the conditional Lyapunov exponent near $\lambda=\sigma=0$, by taking the derivative of Eq. (65) with respect to λ and then setting $\lambda=0$:

$$\left.\frac{d\sigma}{d\lambda}\right|_{\lambda=0}=\frac{2}{v}. \tag{66}$$

We test Eq. (66) through simulation by varying the parameter b_r at a particular value of f_{0r}, so that we cross the threshold of synchronization, measuring the conditional Lyapunov exponent and the distribution exponent along this path. In Fig. 16, we show the relationship between the two measures of synchronization along two paths $f_{0r}=0.35$ and $f_{0r}=0.75$. We measure both σ and λ as they change sign together, and from these measurements calculate the values of $d\sigma/d\lambda|_{\lambda=0}$ shown in column 1 of Table I. We compare the measured values of the slopes with predictions resulting from the use of simulated measurements of v within Eq. (66) shown in column 2 of Table I. Our analytical model can also be used to predict the slope roughly. We approximate v by the variance of the instantaneous Lyapunov exponent which we calculate similarly to Eq. (62),

$$v=\lim_{N\to\infty} N\ \mathrm{var}(\Lambda^N)\approx\mathrm{var}(\Lambda^1)=\int_{-1/2}^{1/2}(\Lambda^1(\theta))^2 f_\Theta(\theta)\,d\theta. \tag{67}$$

These results are contained in column 3 of Table I.

TABLE I. Comparisons of the values of $d\sigma/d\lambda|_{\lambda=0}$ measured from the plot in Fig. 16, the values predicted by Eq. (66) through simulation measurement of v, and the values predicted by Eq. (66) through the approximate predictions of v from analysis.

Condition for $\lambda=\sigma=0$		$\left.\frac{d\sigma}{d\lambda}\right\|_{\lambda=0}$	$\left.\frac{d\sigma}{d\lambda}\right\|_{\lambda=0}$	$\left.\frac{d\sigma}{d\lambda}\right\|_{\lambda=0}$
f_{0r}	b_r	Measured from Simulation	Predicted by v	Predicted from analysis
0.35	0.134	1.4	1.6	2.6
0.75	0.261	0.82	0.91	0.89

VI. CONCLUSION AND DISCUSSION

We used a system of three DPLL's to study chaotic synchronization both experimentally and analytically. One ''feeding'' DPLL produced a chaotic signal which was the input for the other two ''receiving'' DPLL's, which were nearly identical to each other. In certain parameter regimes, we observed synchronization between the two receiving DPLL's. A linear scaling region in a plot of log of probability versus the log of separation gives a measure of the degree of synchronization and the magnitude of the system differences. The slope of this line is the distribution exponent σ which quantifies the degree of synchronization: the more positive the slope, the more the two systems are unsynchronized; the more negative the slope, the more the systems are synchronized.

We compared the degree of synchronization in our experimental DPLL system with the degree of synchronization in the equations that simulate the experiment using the distribution exponent. For the simulation, we also computed the Lyapunov exponent. We developed a model of the DPLL system by replacing the chaotic output of the first DPLL with a random frequency process. We analyzed the synchronization behavior of this model through the conditional Lyapunov exponent, and showed that the results were in good agreement with the numerical simulation. Thus we concluded that the model could be used to approximate the Lyapunov exponent of the simulated system. The conditional Lyapunov exponent of the model was then compared with experimental values of the distribution exponent near the threshold of synchronization, where the theory relates the two measures of synchronization giving reasonable agreement. We concluded that a chaotic input can be replaced by noise for modeling our synchronizing system.

The contour plots of distribution exponent in Figs. 10 and 11 differ most from the contour plots of conditional Lyapunov exponent in Figs. 12 and 15 in the lower right corner of the plots, where the two systems are strongly unsynchronized. This aberration can be overcome by using groups of three or more systems. One can define an average separation for larger numbers of nearly identical systems, and study the behavior of the density function describing this separation [17]. The maximum distribution exponent possible for these larger groups of systems increases beyond unity, and we expect large values of the distribution and conditional Lyapunov exponent to be in closer agreement.

The scope of this paper only encompassed measurement of the synchronization of the two ''receiving'' systems. Because the signal from the feed differs from the output of the receiver, synchronization of the ''receiving'' systems with the ''feeding'' system falls into the realm of generalized syn-

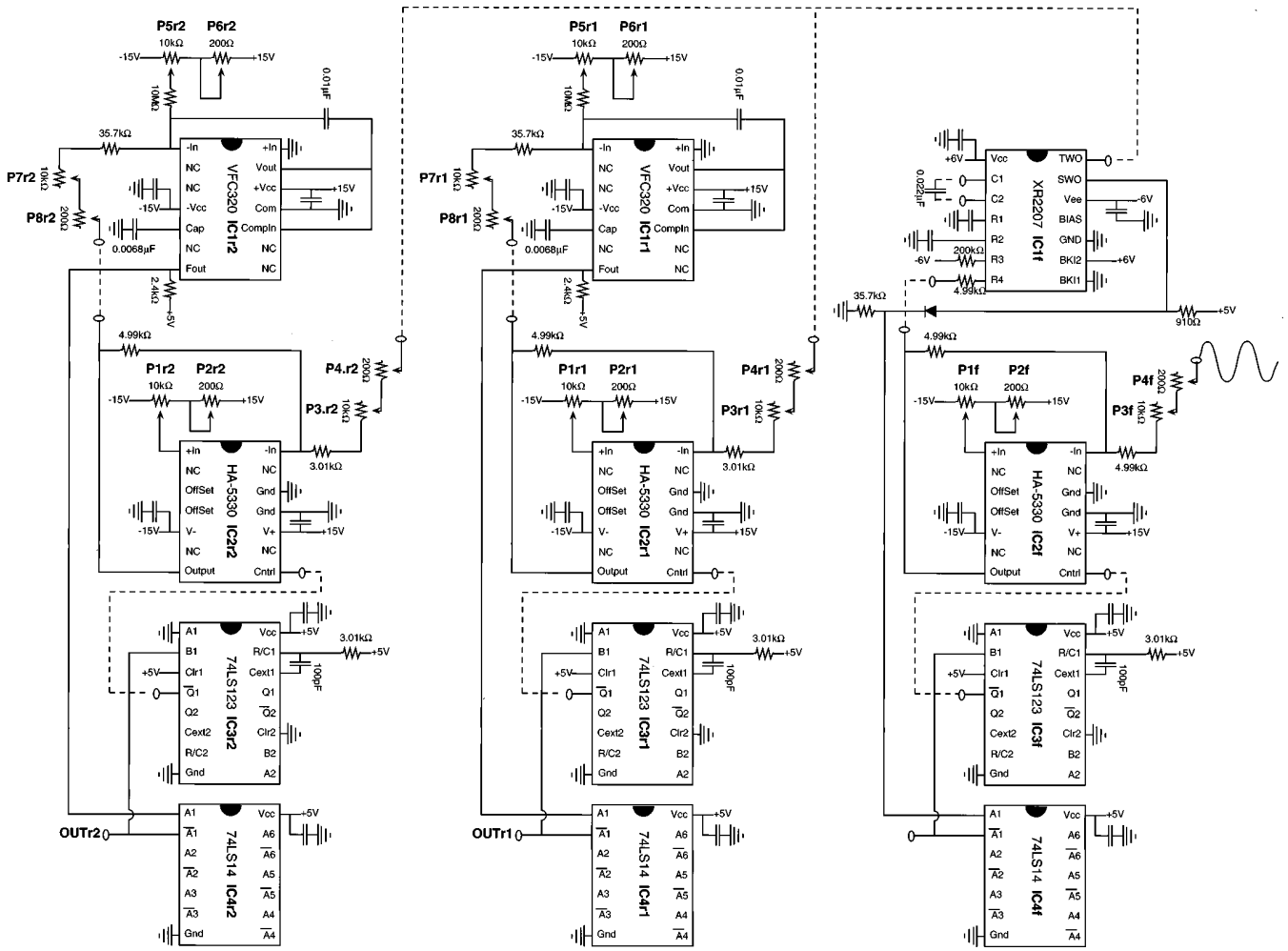

FIG. 17. Experimental circuit diagram. All unlabeled capacitors are bypass capacitors for the power supplies and are 0.1 μF.

chronization, which we did not address. However, our experimental and simulation systems were arranged almost identically to those used by Abarbanel, Rulkov, and Sushchik to measure generalized synchronization using the auxiliary systems approach [4]. They concluded that synchronization of the two ''receiving'' (or response) systems with each other indicates a generalized synchronization of each with the first system. Their new simple test replaces involved computation [3,24]. For experimental measurement of generalized synchronization through the auxiliary systems approach, we propose using the distribution exponent.

ACKNOWLEDGMENTS

We would like to acknowledge Edgar Knobloch, who helped give us the insight about how to analyze the randomly fed DPLL system. This work was partially funded by NSF Grant No. Phy 9505621.

APPENDIX A

Figure 17 shows the full circuit diagram of the experiment. Integrated circuits (IC's) $1f$-$4f$ make up the feeding DPLL and IC's $1r$-$4r$ make up the receiving DPLL's. The VCO's (IC1) produce triangular waves. The voltage frequency characteristics of IC's $1r$ are ultralinear, but the triangular waves produced are not symmetric like those of IC $1f$. The voltage that determines the frequency of this wave comes from a sample and hold amplifier (IC2). The parameters of all DPLL's are tuned by using the potentiometers ($P1-P4$) attached to IC2. $P1$ and $P2$ change f_0, while $P3$ and $P4$ change b. When the control input of ICZ is low it samples and when the input is high, the IC holds the applied voltage. Our model [Eqs. (23) and (24)] assumes that an instantaneous sample is taken. This is approximated using a one-shot integrated circuit IC3. The pulse generated by this circuit goes low for 0.87 μs, which is only 0.1% of a typical oscillation period, and results in a sample within 0.1% of the true value. IC4, which triggers a pulse in the one shot, is fed by the square wave output of the VCO (IC1), and sharpens the leading edge of this signal eliminating VCO noise which might make that transition ambiguous.

Operation of the circuit at a particular point in the $f_{0f}b_f f_{0r}b_r$ parameter space requires careful adjustment of all the potentiometers ($P1-P8$) in the diagram. To tune the circuit before operation we remove all dashed input connections, so that known voltages can be applied to the VCO, and voltage to frequency characteristics can be accurately measured. By measuring the voltage to frequency characteristics of the two VFC320's and adjusting the potentiometers ($P5r-P8r$), we match those characteristics to those shown in Fig. 6(a). More importantly, we adjust the voltage fre-

quency characteristics of the VFO320's to be nearly identical to each other as shown in Fig. 6(b). Next the VCO (IC1r) is reconnected to the SH (IC2r). We measure the range of the input signal $g_c(t)$ to IC2r, which comes from IC1f. The lowest voltage in this range typically 2.4 V should produce a frequency of $f_{0r}-b_r$, while the highest voltage, typically 9.6 V, should produce a frequency of $f_{0r}+b_r$. By adjusting the potentiometers $P1r1-P4r1$ and applying the known upper and lower voltages in the input range, we tune the first ''receiving'' DPLL to the parameters f_{0r}^1 and b_r^1. By adjusting $P1r2-P4r2$ we assure that the two amplifiers differ from each other by much less than one part in 1000 and that $f_{0r}^1 \approx f_{0r}^2$ and $b_r^1 \approx b_r^2$. Once all of the dashed wires are reconnected, the circuit operates at the desired point in parameter space.

To make measurements of the synchronization behavior of this circuit we use a data acquisition board made by National Instruments. An on-board 10-MHz clock runs two counters, each of which has an input from OUT $r1$ and OUT $r2$. When these inputs go from low to high, the computer reads the value of the counters, which measure to within 0.1 μs when the two DPLL loops sampled. Labview software is then used to process this data.

APPENDIX B

We show that the maximum value for the distribution exponent between two systems is unity by considering two systems on the circle $[-\frac{1}{2},\frac{1}{2})$ which are completely unsynchronized. We model these two systems with random variables. The states w and x of the two systems w are represented by the random variables W and X, respectively, which are uniformly distributed between $[-\frac{1}{2},\frac{1}{2})$. We assume that the two random variables W and X are independent of one another. The linear difference r between the two random variables is the random variable R,

$$R=|X-W|, \tag{B1}$$

defined on the circle $[-\frac{1}{2},\frac{1}{2})$, such that any differences that fall outside $[-\frac{1}{2},\frac{1}{2})$ are mapped back into the interval through identification of the integer multiples. The largest separation r that can occur between w and x is $\frac{1}{2}$. The density function of r is uniformly distributed between $[0,\frac{1}{2}]$,

$$f_R(r)=2, \quad 0\leqslant r\leqslant \tfrac{1}{2}. \tag{B2}$$

Defining a new random variable Z,

$$Z=\ln(R), \tag{B3}$$

and transforming Eq. (B2), we obtain

$$f_Z(z)=2e^z, \quad z\leqslant \ln(\tfrac{1}{2}). \tag{B4}$$

Taking the logarithm of Eq. (B4) gives

$$\ln(f_Z(z))=\ln(2)+z, \quad z\leqslant \ln(\tfrac{1}{2}). \tag{B5}$$

The slope of $\ln(f_Z(z))$ vs z, which is the distribution exponent, is unity.

APPENDIX C

At one sampling instant of the receiving DPLL, we assume the phase $\theta(0)$ of the feeding signal to be a sure variable with fixed value, and the frequency of the signal $F(0)$ to be a random variable with the Ornstein-Uhlenbeck steady state distribution. In steady state the frequency $F(0)$ of the feeding signal at the time of the sample is a normally distributed random variable with mean f_{0f} and variance A. We decompose this into the average frequency f_{0f}, which is a sure variable, and the change from that average $\Delta F(0)$, which is a normal random variable with mean 0 and variance A:

$$F(0)=f_{0f}+\Delta F(0). \tag{C1}$$

After a length of time Δt,

$$\Delta t=t_{n+1}-t_n=\frac{1}{f_{0r}(1+b_r\psi_n)}=\frac{1}{f_{0r}(1+b_r g_f(\theta))}, \tag{C2}$$

a new sample of the DPLL is taken at a phase given by the random variable $\Theta(\Delta t)$, which depends on both the phase $\theta(0)$ and the frequency $F(0)$ of the initial sample. The average value of Θ is

$$\langle\Theta(\Delta t)\rangle=\langle\langle\Theta(\Delta t)\rangle_{\Theta(\Delta t)}\rangle_{F(0)}, \tag{C3}$$

where the expectation is over the phase variable and the random frequency variable $F(0)$ and is a function of the sampled phase $\theta(0)$. To determine this expectation, we condition the inner expectation on $F(0)$ by assuming that we know the value of the random variable $\Delta F(0)$ to be $\Delta f(0)$, a fixed value:

$$\langle\langle\Theta(\Delta t)\rangle_{\Theta(\Delta t)}\rangle_{F(0)}=\langle\langle\Theta(\Delta t)|\Delta F(0)=\Delta f(0)\rangle_{\Theta(\Delta t)}\rangle_{F(0)}. \tag{C4}$$

We decompose the random phase $\Theta(\Delta t)$ into its previous value $\theta(0)$, the constant increase $\Delta\theta_0(\Delta t)$ due to the average frequency which is not random, and the random deviation of phase $\Delta\Theta(\Delta t)$:

$$\Theta(\Delta t)=\theta(0)+\Delta\theta_0(\Delta t)+\Delta\Theta(\Delta t). \tag{C5}$$

The second term on the right side results from the average frequency f_{0f} and is the fixed function

$$\Delta\theta_0(\Delta t)=f_{0f}\Delta t. \tag{C6}$$

We substitute Eq. (C6) into Eq. (C5), and take the conditional expectation

$$\begin{aligned}\langle\Theta(\Delta t)|\Delta F(0)=\Delta f(0)\rangle_{\Theta(\Delta t)} &=\langle\theta(0)|\Delta F(0)=\Delta f(0)\rangle+\langle f_{0f}\Delta t|\Delta F(0)=\Delta f(0)\rangle \\ &\quad+\langle\Delta\Theta(\Delta t)|\Delta F(0)=\Delta f(0)\rangle.\end{aligned} \tag{C7}$$

The first two terms on the right hand side are sure variables, so we can drop those expectations. The third term on the

right hand side is the integral of the random process $\Delta F(t)$. This average for the Ornstein-Uhlenbeck process is [23]

$$\langle \Delta\Theta(\Delta t)|\Delta F(0)=\Delta f(0)\rangle_{\Theta(\Delta t)}=\Delta f(0)\,\tau(1-e^{-\Delta t/\tau}). \tag{C8}$$

Equation (C7) simplifies to

$$\langle \Theta(\Delta t)|\Delta F(0)=\Delta f(0)\rangle_{\Theta(\Delta t)} = \theta(0)+f_{0f}\Delta t+\Delta f(0)\,\tau(1-e^{-\Delta t/\tau}) \tag{C9}$$

We now take the expectation over $\Delta F(0)$, which is the same as taking the expectation over $F(0)$,

$$\langle\langle \Theta(\Delta t)|\Delta F(0)=\Delta f(0)\rangle_{\Theta(\Delta t)}\rangle_{\Delta F(0)} = \theta+f_{0f}\Delta t+\langle \Delta F(0)\rangle_{\Delta F(0)}\tau(1-e^{-\Delta t/\tau}). \tag{C10}$$

Because $\Delta F(0)$ is a normal random variable with mean zero,

$$\langle \Delta F(0)\rangle_{\Delta F(0)}=0. \tag{C11}$$

Hence Eq. (C10) simplifies to

$$\langle \Theta(\Delta t)\rangle=\theta+f_{0f}\Delta t. \tag{C12}$$

To obtain the variance

$$\langle \Theta(\Delta t)^2\rangle-\langle \Theta(\Delta t)\rangle^2=\langle\langle \Theta(\Delta t)^2\rangle_{\Theta(\Delta t)}\rangle_{F(0)} -\langle\langle \Theta(\Delta t)\rangle_{\Theta(\Delta t)}\rangle^2_{F(0)}, \tag{C13}$$

note that from Eq. (C12)

$$\langle \Theta(\Delta t)\rangle^2=(\theta+f_{0f}\Delta t)^2. \tag{C14}$$

We take the conditional expectation of the left term,

$$\langle \Theta(\Delta t)^2\rangle=\langle\langle \Theta(\Delta t)^2|\Delta F(0)=\Delta f(0)\rangle_{\Theta(\Delta t)}\rangle_{\Delta F(0)}. \tag{C15}$$

The inner expectation is related to the variance through

$$\langle \Theta(\Delta t)^2|\Delta F(0)=\Delta f(0)\rangle_{\Theta(\Delta t)} =\langle \Theta(\Delta t)|\Delta F(0)=\Delta f(0)\rangle^2_{\Theta(\Delta t)} +\mathrm{var}\{\Theta(\Delta t)|\Delta F(0)=\Delta f(0)\}_{\Theta(\Delta t)}. \tag{C16}$$

The first term on the right side is evaluated using Eq. (C9),

$$\langle \Theta(\Delta t)|\Delta F(0)=\Delta f(0)\rangle^2_{\Theta(\Delta t)} =(\theta+f_{0f}\Delta t)^2+2(\theta+f_{0f}\Delta t)\Delta f(0)\,\tau(1-e^{-\Delta t/\tau}) +[\Delta f(0)\,\tau(1-e^{-\Delta t/\tau})]^2. \tag{C17}$$

The second term of Eq. (C16) is a standard characteristic of the Ornstein-Uhlenbeck process [23],

$$\mathrm{var}\{\Theta(\Delta t)|\Delta F(0)=\Delta f(0)\}_{\Theta(\Delta t)} =2A\tau\left[\Delta t-2\tau(1-e^{-\Delta t/\tau})+\frac{\tau}{2}(1-e^{-2(\Delta t/\tau)})\right]. \tag{C18}$$

Substituting Eqs. (C17) and (C18) into Eq. (C16), and taking the expectation of $\Delta F(0)$, gives

$$\begin{aligned}\langle\langle \Theta(\Delta t)^2|\Delta F(0)=\Delta f(0)\rangle_{\Theta(\Delta t)}\rangle_{\Delta F(0)} &=(\theta+f_{0f}\Delta t)^2+2(\theta+f_{0f}\Delta t)\\ &\quad\times\langle \Delta F(0)\rangle_{\Delta F(0)}\tau(1-e^{-\Delta t/\tau})\\ &\quad+\langle \Delta F(0)^2\rangle_{\Delta F(0)}\tau^2(1-e^{-\Delta t/\tau})^2\\ &\quad+2A\tau\left[\Delta t-2\tau(1-e^{-\Delta t/\tau})\right.\\ &\quad\left.+\frac{\tau}{2}(1-e^{-2(\Delta t/\tau)})\right].\end{aligned} \tag{C19}$$

The steady state implies Eq. (C11), and also implies that

$$\langle \Delta F(0)^2\rangle_{\Delta F(0)}=A. \tag{C20}$$

Substituting Eqs. (C11) and (C20) into Eq. (C19) gives

$$\begin{aligned}\langle\langle \Theta(\Delta t)^2|\Delta F(0)=\Delta f(0)\rangle_{\Theta(\Delta t)}\rangle_{\Delta F(0)} &=(\theta+f_{0f}\Delta t)^2+A\tau^2(1-e^{-\Delta t/\tau})^2\\ &\quad+2A\tau\left[\Delta t-2\tau(1-e^{-\Delta t/\tau})\right.\\ &\quad\left.+\frac{\tau}{2}(1-e^{-2\Delta t/\tau})\right],\end{aligned} \tag{C21}$$

We substitute Eqs. (C14) and (C21) into Eq. (C13), and simplify, to determine the variance

$$\langle \Theta(\Delta t)^2\rangle-\langle \Theta(\Delta t)\rangle^2=2A\tau(\Delta t-\tau+\tau e^{-\Delta t/\tau}). \tag{C22}$$

Equations (C12) and (C22) are the mean and variance of a Gaussian random variable, and together they specify the probability distribution of phase of a new sample of the random frequency input signal.

APPENDIX D

To determine the coefficients t more easily, we decompose the stochastic map of Eqs. (39) and (40) into two steps: stochastic and nonstochastic. Consider the nth sample to be the sure variable θ_n. The first step of the map is nonstochastic, and maps the sure variable θ_n to a new sure variable θ_{n+1} as dictated by Eq. (39). This is a simple transformation. The second, stochastic, step spreads the sure variable θ_{n+1} into the random variable Θ_{n+1}. Because the new random variable Θ_{n+1} is the integral of a Gaussian random process, it is normally distributed with mean θ_{n+1} and variance v, which are functions of θ through Eqs. (39) and (40). We can view Θ_{n+1} as arising from the addition of the sure variable θ_{n+1}, and the random variable Ξ, which is normally distributed with the same variance v as Θ_{n+1} but with mean 0. The nth sample is not sure, but instead is the random variable Θ_n

which is distributed with density function $f_{\Theta_n}(\theta)$.

We express $f_{\Theta_n}(\theta)$ in terms of its Fourier series

$$f_{\Theta_n}(\theta)=\frac{a_0}{2}+\sum_{n=1}^{\infty} a_n\cos(2\pi n\theta)+\sum_{n=1}^{\infty} b_n\sin(2\pi n\theta). \tag{D1}$$

The coefficients a_n and b_n are determined through

$$a_n=2\int_{-1/2}^{1/2} f_{\Theta_n}(\theta)\cos(2\pi n\theta)\,d\theta \tag{D2}$$

and

$$b_n=2\int_{-1/2}^{1/2} f_{\Theta_n}(\theta)\sin(2\pi n\theta)\,d\theta. \tag{D3}$$

The distribution of this random variable after mapping by the nonstochastic step of the map is defined to be $f'_{\Theta'_n}(\theta')$ which terms of a Fourier series, is

$$f'_{\Theta'_n}(\theta')=\frac{a'_0}{2}+\sum_{n=1}^{\infty} a'_n\cos(2\pi n\theta')+\sum_{n=1}^{\infty} b'_n\sin(2\pi n\theta'). \tag{D4}$$

Likewise, we define the distribution after both the nonstochastic and stochastic map steps as $f''_{\Theta_{n+1}}(\theta'')$, and express it in terms of the Fourier series

$$f''_{\Theta_{n+1}}(\theta'')=\frac{a''_0}{2}+\sum_{n=1}^{\infty} a''_n\cos(2\pi n\theta'')+\sum_{n=1}^{\infty} b''_n\sin(2\pi n\theta''). \tag{D5}$$

The last Fourier series required is that for the normally distributed random variable used in the stochastic step of the noisy map Ξ. While the domains of the density functions f are the circle, the domain of the Gaussian density function defining the stochastic step of the map is the real line. We map numbers from the real line to the circle by identifying all numbers separated by integers. This identification transforms

$$f_{\Xi}(v,\xi')=\frac{1}{\sqrt{2\pi v}}\,e^{-\xi'^2/2v}, \tag{D6}$$

defined over the real line into

$$f_{\Xi}(v,\xi)=\sum_{i=-\infty}^{\infty}\frac{1}{\sqrt{2\pi v}}\,e^{-(\xi+i)^2/2v} \tag{D7}$$

defined over the circle. Because this random variable depends on v, its density function depends on v,

$$f_{\Xi}(v,\xi)=\frac{\xi_0^a(v)}{2}+\sum_{m=1}^{\infty}\xi_m^a(v)\cos(2\pi m\xi)+\sum_{m=1}^{\infty}\xi_m^b(v)\sin(2\pi m\xi), \tag{D8}$$

and in turn the Fourier coefficients of the density function depend on v:

$$\xi_m^a(v)=2\int_{-1/2}^{1/2} f_{\Xi}(v,\xi)\cos(2\pi m\xi)\,d\xi \tag{D9}$$

and

$$\xi_m^b(v)=2\int_{-1/2}^{1/2} f_{\Xi}(v,\xi)\sin(2\pi m\xi)\,d\xi. \tag{D10}$$

If we use Eq. (D7) in Eqs. (D9) and (D10), the integrals can be evaluated by exchanging the order of integration and summation:

$$\xi_m^a(v)=2\sum_{i=-\infty}^{\infty}\left(\int_{[i-(1/2)]}^{[i+(1/2)]}\frac{1}{\sqrt{2\pi v}}\,e^{-\xi^2/2v}\cos(2\pi m\xi)\,d\xi\right) \tag{D11}$$

and

$$\xi_m^b(v)=2\sum_{i=-\infty}^{\infty}\left(\int_{[i-(1/2)]}^{[i+(1/2)]}\frac{1}{\sqrt{2\pi v}}\,e^{-\xi^2/2v}\sin(2\pi m\xi)\,d\xi\right). \tag{D12}$$

We obtain the results

$$\xi_m^a(v)=2\int_{-\infty}^{\infty}\frac{1}{\sqrt{2\pi v}}\,e^{-\xi^2/2v}\cos(2\pi m\xi)\,d\xi=2e^{-2\pi^2m^2v} \tag{D13}$$

and

$$\xi_m^b(v)=2\int_{-\infty}^{\infty}\frac{1}{\sqrt{2\pi v}}\,e^{-\xi^2/2v}\sin(2\pi m\xi)\,d\xi=0. \tag{D14}$$

The random variable θ'' is the sum of two random variables θ' and Ξ. The density function of the sum of two random variables is the convolution of the individual density functions

$$f''_{\Theta_{n+1}}(\theta'')=\int_{-1/2}^{1/2} f_{\Xi}(v,\theta''-\theta')f'_{\Theta'_n}(\theta')\,d\theta'. \tag{D15}$$

We use the expression

$$a''_n=2\int_{-1/2}^{1/2} f''_{\Theta_{n+1}}(\theta'')\cos(2\pi n\theta'')\,d\theta'', \tag{D16}$$

for a''_n together with Eq. (D15) to yield

$$a''_n=2\int_{-1/2}^{1/2}\left\{\int_{-1/2}^{1/2} f_{\Xi}(v,\theta''-\theta')f'_{\Theta'_n}(\theta')\,d\theta'\right\}\times\cos(2\pi n\theta'')\,d\theta''. \tag{D17}$$

Because all functions within both integrals are periodic, we interchange the order of the integrals

$$a_n'' = 2\int_{-1/2}^{1/2}\left\{\int_{-1/2}^{1/2} f_\Xi(v,\theta''-\theta')\cos(2\pi n\theta'')\,d\theta''\right\} \times f'_{\Theta'_n}(\theta')\,d\theta'. \tag{D18}$$

We examine just the term in brackets substituting Eq. (D8) for $f_\Xi(v,\xi)$:

$$\begin{aligned}\int_{-1/2}^{1/2} f_\Xi(v,\theta''-\theta')\cos(2\pi n\theta'')\,d\theta'' &= \int_{-1/2}^{1/2}\frac{\xi_0^a(v)}{2}\cos(2\pi n\theta'')\,d\theta'' \\ &+ \int_{-1/2}^{1/2}\left(\sum_{m=1}^{\infty}\xi_m^a(v)\cos(2\pi m(\theta''-\theta'))\right) \\ &\times\cos(2\pi n\theta'')\,d\theta'' \\ &+ \int_{-1/2}^{1/2}\left(\sum_{m=1}^{\infty}\xi_m^b(v)\sin(2\pi m(\theta''-\theta'))\right) \\ &\times\cos(2\pi n\theta'')\,d\theta''.\end{aligned} \tag{D19}$$

From Eq. (D14), the third term on the right hand side is zero:

$$\begin{aligned}\int_{-1/2}^{1/2} f_\Xi(v,\theta''-\theta')\cos(2\pi n\theta'')\,d\theta'' &= \int_{-1/2}^{1/2}\frac{\xi_0^a(v)}{2}\cos(2\pi n\theta'')\,d\theta'' \\ &+ \int_{-1/2}^{1/2}\left(\sum_{m=1}^{\infty}\xi_m^a(v)\cos(2\pi m(\theta''-\theta'))\right) \\ &\times\cos(2\pi n\theta'')\,d\theta''.\end{aligned} \tag{D20}$$

We interchange the order of integration and summation

$$\begin{aligned}\int_{-1/2}^{1/2} f_\Xi(v,\theta''-\theta')\cos(2\pi n\theta'')\,d\theta'' &= \frac{\xi_0^a(v)}{2}\int_{-1/2}^{1/2}\cos(2\pi n\theta'')\,d\theta'' \\ &+ \sum_{m=1}^{\infty}\xi_m^a(v)\int_{-1/2}^{1/2}\cos(2\pi m(\theta''-\theta')) \\ &\times\cos(2\pi n\theta'')\,d\theta''.\end{aligned} \tag{D21}$$

Because of the orthogonality of sinusoidal integrals, Eq. (D21) can be greatly simplified. We introduce the Kroenecker delta

$$\delta_{nm} = \begin{cases} 1, & n=m \\ 0, & n\neq m. \end{cases} \tag{D22}$$

The first integral on the right hand side is

$$\int_{-1/2}^{1/2}\cos(2\pi n\theta'')\,d\theta'' = \delta_{n0}. \tag{D23}$$

The second integral is

$$\int_{-1/2}^{1/2}\cos(2\pi m(\theta''-\theta'))\cos(2\pi n\theta'')\,d\theta'' = \delta_{nm}\frac{\cos(2\pi n\theta')}{2}. \tag{D24}$$

Taking Eqs. (D23) and (D24), substituting into Eq. (D21), and carrying out the sums, gives

$$\begin{aligned}\int_{-1/2}^{1/2} f_\Xi(v,\theta''-\theta')\cos(2\pi n\theta'')\,d\theta'' &= \begin{cases}\dfrac{\xi_0^a(v)}{2}, & n=0 \\ \xi_n^a(v)\dfrac{\cos(2\pi n\theta')}{2}, & n\neq 0.\end{cases}\end{aligned} \tag{D25}$$

But

$$\frac{\xi_0^a(v)}{2} = \xi_n^a(v)\frac{\cos(2\pi n\theta')}{2}, \quad n=0, \tag{D26}$$

so we simplify Eq. (D25) to

$$\int_{-1/2}^{1/2} f_\Xi(v,\theta''-\theta')\cos(2\pi n\theta'')\,d\theta'' = \xi_n^a(v)\frac{\cos(2\pi n\theta')}{2}. \tag{D27}$$

Substituting Eq. (D27) into Eq. (D18) gives

$$a_n'' = \int_{-1/2}^{1/2}\xi_n^a(v)\cos(2\pi n\theta')f'_{\Theta'_n}(\theta')\,d\theta'. \tag{D28}$$

We transform from the variable θ' to the variable θ using the nonstochastic map (39), $\theta' = \langle\Theta(\theta)\rangle$.

The variable substitution works smoothly because the probability density and the differentials transform from one variable to another as [22]

$$f'_{\Theta'_n}(\theta')\,d\theta' = f_{\Theta_n}(\theta)\,d\theta. \tag{D29}$$

Carrying out the substitution, we have

$$a_n'' = \int_{\langle\Theta(-1/2)\rangle^{-1}}^{\langle\Theta(1/2)\rangle^{-1}}\xi_n^a(v)\cos[2\pi n\langle\Theta(\theta)\rangle]f_{\Theta_n}(\theta)\,d\theta. \tag{D30}$$

Because the integrand, the function $\langle\Theta(\theta)\rangle$, the variable θ'', and the variable θ are all on the circle and periodic with period 1, we shift the limits of Eq. (D30) to run from $-\frac{1}{2}$ to $\frac{1}{2}$,

$$a_n'' = \int_{-1/2}^{1/2}\xi_n^a(v)\cos(2\pi n\langle\Theta(\theta)\rangle)f_{\Theta_i}(\theta)\,d\theta. \tag{D31}$$

To determine the relation between the fourier coefficients of the distribution of one sample and the next, we substitute Eq. (D1) into Eq. (D31) changing the variable of summation in Eq. (D1) to m

$$a_n'' = \int_{-1/2}^{1/2} \xi_n^a(v)\cos(2\pi n\langle\Theta(\theta)\rangle) \times\left(\frac{a_0}{2}+\sum_{m=1}^{\infty} a_m\cos(2\pi m\theta) + \sum_{m=1}^{\infty} b_m\sin(2\pi m\theta)\right)d\theta. \quad \text{(D32)}$$

We interchange the order of the integration and summation,

$$a_n'' = \left(\int_{-1/2}^{1/2}\xi_n^a(v)\,\frac{\cos[2\pi n\langle\Theta(\theta)\rangle]}{2}\,d\theta\right)a_0 + \sum_{m=1}^{\infty}\left(\int_{-1/2}^{1/2}\xi_n^a(v)\cos[2\pi n\langle\Theta(\theta)\rangle] \times\cos(2\pi m\theta)d\theta\right)a_m + \sum_{m=1}^{\infty}\left(\int_{-1/2}^{1/2}\xi_n^a(v)\cos[2\pi n\langle\Theta(\theta)\rangle] \times\sin(2\pi m\theta)d\theta\right)b_m. \quad \text{(D33)}$$

We write all of the dependencies explicitly, substituting Eq. (D13) for the coefficients $\xi_n^a(v)$:

$$a_n'' = \left(\int_{-1/2}^{1/2} 2e^{-2\pi^2m^2v(\theta_i)}\,\frac{\cos(2\pi n\langle\Theta(\theta_i)\rangle)}{2}\,d\theta_i\right)a_0 + \sum_{m=1}^{\infty}\left(\int_{-1/2}^{1/2}2e^{-2\pi^2m^2v(\theta_i)}\cos(2\pi n\langle\Theta(\theta_i)\rangle) \times\cos(2\pi m\theta)d\theta_i\right)a_m + \sum_{m=1}^{\infty}\left(\int_{-1/2}^{1/2}2e^{-2\pi^2m^2v(\theta_i)}\cos(2\pi n\langle\Theta(\theta_i)\rangle) \times\sin(2\pi m\theta)d\theta_i\right)b_m. \quad \text{(D34)}$$

Through similar calculations as Eqs. (D16)–(D34) we find an expression for b_n'':

$$b_n'' = \left(\int_{-1/2}^{1/2} 2e^{-2\pi^2m^2v(\theta_i)}\,\frac{\sin(2\pi n\langle\Theta(\theta_i)\rangle)}{2}\,d\theta_i\right)a_0 + \sum_{m=1}^{\infty}\left(\int_{-1/2}^{1/2}2e^{-2\pi^2m^2v(\theta_i)}\sin(2\pi n\langle\Theta(\theta_i)\rangle) \times\cos(2\pi m\theta)d\theta_i\right)a_m + \sum_{m=1}^{\infty}\left(\int_{-1/2}^{1/2}2e^{-2\pi^2m^2v(\theta_i)}\sin(2\pi n\langle\Theta(\theta_i)\rangle) \times\sin(2\pi m\theta)d\theta_i\right)b_m. \quad \text{(D35)}$$

Equations (D34) and (D35) relate the fourier coefficients of the random variable density function at the time of a sample to the Fourier coefficients of the density function at the time of the next sample. We define the coefficients

$$t_{n0}^{aa} = \int_{-1/2}^{1/2}\xi_n^a(v)\,\frac{\cos(2\pi n\langle\Theta(\theta)\rangle)}{2}\,d\theta, \quad \text{(D36)}$$

$$t_{nm}^{aa} = \int_{-1/2}^{1/2}\xi_n^a(v)\cos(2\pi n\langle\Theta(\theta)\rangle)\cos(2\pi m\theta)d\theta, \quad \text{(D37)}$$

$$t_{nm}^{ab} = \int_{-1/2}^{1/2}\xi_n^a(v)\cos(2\pi n\langle\Theta(\theta)\rangle)\sin(2\pi m\theta)d\theta, \quad \text{(D38)}$$

$$t_{n0}^{ba} = \int_{-1/2}^{1/2}\xi_n^a(v)\,\frac{\sin(2\pi n\langle\Theta(\theta)\rangle)}{2}\,d\theta, \quad \text{(D39)}$$

$$t_{nm}^{ba} = \int_{-1/2}^{1/2}\xi_n^a(v)\sin(2\pi n\langle\Theta(\theta)\rangle)\cos(2\pi m\theta)d\theta, \quad \text{(D40)}$$

and

$$t_{nm}^{bb} = \int_{-1/2}^{1/2}\xi_n^a(v)\sin[2\pi n\langle\Theta(\theta)\rangle]\sin(2\pi m\theta)d\theta, \quad \text{(D41)}$$

and rewrite Eqs. (D34) and (D35) as Eqs. (49) and (50).

[1] L. M. Pecora and T. L. Carroll, Phys. Rev. Lett. **64**, 821 (1990).
[2] L. M. Pecora and T. L. Carroll, Phys. Rev. A **44**, 2374 (1991).
[3] N. F. Rulkov, M. M. Sushchik, L. S. Tsimring, and H. D. I. Abarbanel, Phys. Rev. E **51**, 980 (1995).
[4] H. D. I. Abarbanel, N. F. Rulkov, and M. M. Sushchik, Phys. Rev. E **53**, 4528 (1996).
[5] C. M. Kim, Phys. Rev. E **56**, 3697 (1997).
[6] T. L. Carroll, J. F. Heagy, and L. M. Pecora, Phys. Rev. E **54**, 4676 (1996).
[7] T. Ushio, T. Innami, and S. Kodama, IEICE Trans. Fundam. Electron. Commun. Comput. Sci. **79**, 1689 (1996).
[8] V. Milanovic and M. E. Zaghloul, Int. J. Bifurcation Chaos Appl. Sci. Eng. **6**, 2571 (1996).
[9] D. Y. Tang, R. Dykstra, and N. R. Heckenberg, Phys. Rev. A **54**, 5317 (1996).

[10] M. de Sousa Vieira, A. J. Lichtenberg, and M. A. Lieberman, Int. J. Bifurcation Chaos Appl. Sci. Eng. **1**, 1 (1991).
[11] M. de Sousa Vieira *et al.*, Int. J. Bifurcation Chaos Appl. Sci. Eng. **2**, 645 (1992).
[12] T. Yang and L. O. Chua, Int. J. Bifurcation Chaos Appl. Sci. Eng. **6**, 2653 (1996).
[13] L. Rahman, G. Li, and F. Tian, Opt. Commun. **138**, 91 (1997).
[14] V. Annovazzi-Lodi, S. Donati, and A. Scire, IEEE J. Quantum Electron. **33**, 1449 (1997).
[15] P. Khoury, M. A. Lieberman, and A. J. Lichtenberg, Phys. Rev. E **54**, 3377 (1996).
[16] A. Wolf, J. B. Swift, H. L. Swinney, and J. A. Vastano, Physica D **16**, 285 (1985).
[17] A. S. Pikovsky, Phys. Lett. A **165**, 33 (1992).
[18] Y. Kuramoto and H. Nakao, Phys. Rev. Lett. **78**, 4039 (1997).
[19] G. M. Bernstein and M. A. Lieberman, IEEE Trans. Circuits Syst. **37**, 1164 (1990).
[20] G. M. Bernstein, M. A. Lieberman, and A. J. Lichtenberg, IEEE Trans. Commun. **37**, 1062 (1989).
[21] G. M. Bernstein, Ph.D. dissertation, University of California, Berkeley, CA, 1988 (unpublished).
[22] A. Leon-Garcia, *Probability and Random Processes for Electrical Engineering* (Addison-Wesley, Reading, MA, 1989).
[23] D. T. Gillespie, *Markov Processes: and Introduction for Physical Scientists* (Academic, Boston, MA, 1992).
[24] L. M. Pecora, T. Carroll, and J. Heagy, Phys. Rev. E **52**, 3420 (1995).